geosciences

MDPI

Article

A Holistic Approach for Coastal–Watershed Management on Tourist Islands: A Case Study from Petra–Molyvos Coast, Lesvos Island (Greece)

Stamatia Papasarafianou [1,*], Ilias Siarkos [2], Aliki Gkaifyllia [3], Stavros Sahtouris [3], Giada Varra [4], Antonis Chatzipavlis [3], Thomas Hasiotis [3] and Ourania Tzoraki [3]

[1] Department of Science and Technology, University of Napoli Parthenope, 80143 Napoli, Italy
[2] Department of Civil Engineering, Democritus University of Thrace, 67100 Xanthi, Greece; isiarkos@aegean.gr
[3] Department of Marine Sciences, University of the Aegean, 81100 Mytilene, Greece; alikigaifillia@yahoo.gr (A.G.); s.sahtouris@aegean.gr (S.S.); a.chatzipavlis@marine.aegean.gr (A.C.); hasiotis@marine.aegean.gr (T.H.); rania.tzoraki@aegean.gr (O.T.)
[4] Department of Engineering, University of Napoli Parthenope, 80143 Napoli, Italy; giada.varra@uniparthenope.it
* Correspondence: stamatia.papasarafianou001@studenti.uniparthenope.it; Tel.: +30-6981-718-533

Abstract: Shoreline configurations are a complex outcome of the dynamic interplay between natural forces and human actions. This interaction shapes unique coastal morphologies and affects sediment transport and erosion patterns along the coastline. Meanwhile, ephemeral river systems play a vital role in shaping coastlines and maintaining ecosystem sustainability, especially in island settings. In this context, the present study seeks to develop a holistic approach that views coast and watershed systems as a continuum, aiming to investigate their relationships in an island environment, while accounting for human interventions in the river regime. For this task, the empirical USLE method was employed to quantify sediment production and transport from the catchment area to the coast, while hydraulic simulations using HEC-RAS were conducted to assess sediment retention within flood-affected areas. Moreover, coastal vulnerability to erosion was evaluated by applying the InVEST CVI model in order to identify areas at risk from environmental threats. The coastal zone of Petra–Molyvos, Lesvos, Greece, was selected as the study area due to ongoing erosion issues, with particular emphasis on its interaction with the Petra stream as a result of significant human intervention at its mouth. According to the study's findings, the examined coastal zone is highly vulnerable to combined erosion from wind and waves, while the river's mouth receives only a small amount of sediment from water fluxes. Evidently, this leads to an increase in beach retreat phenomena, while highlighting the necessity for integrated coastal–watershed management.

Keywords: coastal vulnerability; water and sediment fluxes; sediment retention; human intervention; integrated coastal–watershed management; NE Aegean Sea; Greece

check for updates

Citation: Papasarafianou, S.; Siarkos, I.; Gkaifyllia, A.; Sahtouris, S.; Varra, G.; Chatzipavlis, A.; Hasiotis, T.; Tzoraki, O. A Holistic Approach for Coastal–Watershed Management on Tourist Islands: A Case Study from Petra–Molyvos Coast, Lesvos Island (Greece). *Geosciences* **2024**, *14*, 326. https://doi.org/10.3390/geosciences14120326

Academic Editor: Sabina Porfido

Received: 27 July 2024
Revised: 22 November 2024
Accepted: 24 November 2024
Published: 2 December 2024

Copyright: © 2024 by the authors. Licensee MDPI, Basel, Switzerland. This article is an open access article distributed under the terms and conditions of the Creative Commons Attribution (CC BY) license (https://creativecommons.org/licenses/by/4.0/).

1. Introduction

Coastal areas are dynamic socio-economic systems that constitute a fundamental part of global financial services; as a matter of fact, coastal services account for approximately 43% of the overall contributions to human well-being [1–5]. These areas provide cultural and ecosystem services, including food provision, recreation activities, and environmental conservation [2–6]. At the same time, island beaches are the most significant tourist destinations, due to the unique ecosystem, beautiful landscape, and cultural attractions. Island coastal areas cover the 3S (Sea–Sun–Sand) tourism model [2,3,7], thus being an important economic source at both local and regional scales [2], e.g., Greek islands (Chios, Lesvos, Rhodes) and Caribbean small islands (Antigua and Barbuda) [3,8–10].

Tourist developments typically occur as close to the beach as possible, often with minimal regulation of the coastal environment. Human activities, such as poorly designed

coastal structures, dredging, coastal vegetation clearing, and excessive groundwater extraction from coastal aquifers, are some of the major pressures on coastal evolution [4,11]. Coastal morphology, however, is affected by changes due to interactions between both human activities and natural processes [11]. From the environmental perspective, natural activities that play a crucial role in coastal areas include tidal movements, wave action, currents, and sea level changes [4,10,11]. All the aforementioned factors collectively shape coastal morphology, while often leading to temporary or permanent shoreline retreat and coastal erosion [5,10,11].

Meanwhile, coastal areas are strongly impacted by water and sediment fluxes from inland river watersheds, particularly those resulting from channelized stream flow [5,11]; in fact, it is estimated that stream flows produce 95% of sediment delivered to the sea [11]. Sediment transport by river systems shows great spatial interactivity with coastlines, constituting the link between terrestrial and marine environments, while maintaining the sediment balance within the entire ecosystem [11–13]. In addition, sediment retention in floodplains is crucial for river geomorphological evolution and has a profound impact on coastal morphology as well [11]. It then becomes clear that understanding the interplay between river and coastal morphology is essential for managing coastal environments and mitigating the impacts of natural and anthropogenic forces.

In particular, when human activities are introduced into the coast–watershed system, their impact on sediment transport can be significantly negative compared to natural processes [11]. Anthropogenic activities, such as river damming, mining, channelization, flood control, and land use changes, are among the most significant factors contributing to reduced sediment supply to coastal zones [14,15]. In this context, human alterations to sediment dynamics and build-up can have important consequences on both coastal and riverine environments, affecting everything from ecosystem health to coastal stability, while increasing coastal erosion phenomena [11,16].

Coastal erosion is widely recognized as a major environmental issue globally due to its immediate and destructive impacts on coastal areas [17,18]. In regions with limited tidal ranges and offshore currents, the shoreline is not naturally enriched with sediments [11]. Instead, fluvial sediment is supplied to coastal zones, particularly during the wet season, to help maintain coastal morphology [19,20]. For instance, intermittent river flow is the primary sediment supply dynamic for the Greek Archipelago, affecting about 18% of its beaches [7]. Consequently, coastal erosion is especially concerning for island beaches due to their limited sediment supply and increased vulnerability to waves, currents, and storms, making them critical "hotspots" for establishing adaptation strategies and frameworks [7,12].

Addressing sediment supply, coastal vulnerability, and river management together can lead to effective and informed solutions, which are essential for maintaining coastal stability and mitigating erosion [21–23]. Coastal protection and conservation require a holistic approach that addresses the multifaceted challenges of coastal management, such as Integrated Coastal Zone Management (ICZM) [24,25]. By adopting ICZM, various sectors can effectively align their needs and concerns, ensuring the sustainable and integrated management of coastal areas [6,26]. Despite numerous investigations and monitoring studies of coastal areas and watersheds, there remains a tendency to view these systems as distinct entities [11,21]. However, it is crucial to consider the watershed and coastal systems as a unified entity, commonly referred to as the "Coast-Watershed Continuum" (CWC) [10,27].

To date, few studies (e.g., [11,28,29]) have provided a holistic approach to coastal–watershed management worldwide, generally leading to a lack of information regarding the connection between coasts and watersheds [11]. In this context, this study aims to develop a multifaceted methodological framework in an attempt to improve the understanding of the interconnection between watersheds and coastal areas, with a specific focus on tourist destinations, while also considering the impact of human activities on the natural environment. To achieve this, various data from a diverse range of sources,

including oceanographic, geomorphological, and hydrological information, were collected, and several well-established methods were utilized. Specifically, this study employed the InVEST Coastal Vulnerability model and the empirical USLE method, as well as hydrological and hydraulic models (including the rational method and HEC-RAS) to examine the interactions between rivers, land, and sea, and integrate multiple processes into a cohesive framework. Through this approach, a more robust and reliable analysis of the relationships between coastal and terrestrial environments can be accomplished.

2. Materials and Methods

2.1. Study Area

Lesvos Island, Greece (Figure 1a), with a coastline extending nearly 320 km [10], contains 217 beaches that collectively cover an area of approximately 1.9 km^2 [10]. Petra–Molyvos beach, located in northwest Lesvos (Figure 1a), was selected as the study area due to its status as the most populous region in the West Lesvos Municipality [30] and its significant annual influx of tourists. Additionally, Monioudi et al. [2] examined numerous coastlines in the Aegean Sea, identifying 3234 beaches that are vulnerable to storm surges and sea level rise. These vulnerabilities are related to the following: (i) narrow beach widths, with around 59% having a maximum width of less than 20 m; (ii) limited terrestrial sediment supply; (iii) extensive coastal development; and (iv) minimal coastal protection. Petra–Molyvos beach reflects several of these characteristics [2,7].

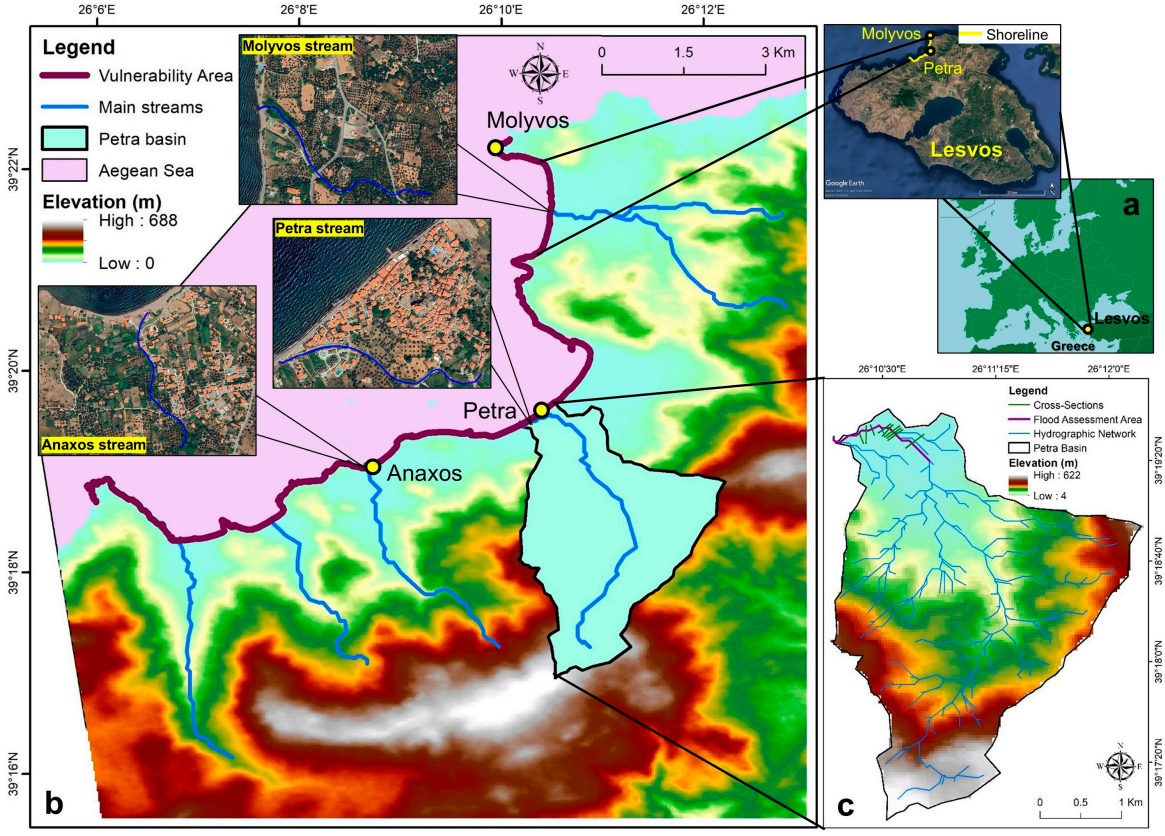


Figure 1. (**a**) A location map of Lesvos Island, Greece, and Petra–Molyvos beach, (**b**) the coastal area, referred to as the "Vulnerability area", where the vulnerability assessment was conducted (including topographic details), along with the main streams interacting with the coast, the mouths of the most significant streams such as Molyvos, Petra, and Anaxos rivers, and the boundaries of the Petra hydrological basin, which was included in the study analysis, and (**c**) topographic and hydrological details of the Petra basin, together with the area referred to as the "Flood Assessment Area", where flood risk assessment was performed.

Furthermore, the beach under study, referred to as the "Vulnerability area" in Figure 1b, has been identified as a "hotspot" primarily due to the following: (a) limited sediment supply from onshore processes (intermittent flow streams, Figure 1b), which, combined with sea waves and forces generated by prevailing winds, increases the risk of beach erosion [7,12] and contributes to beach retreat phenomena [2,7,31]; and (b) human interventions such as the expansion of land use (both agricultural and urban development for recreational activities) and stream channelization, which raise the risk of flooding.

Among the various intermittent flow streams interacting with the coast (Figure 1b), the Molyvos, Anaxos, and Petra streams are recognized as the most significant in terms of sediment supply, with the Petra stream being the most important, especially when accounting for human intervention. As illustrated in Google Earth images of the mouths of the three rivers mentioned above (Figure 1b), a larger section of the Petra River has been channelized compared to the others, while human activities, particularly residential development, are more pronounced near its mouth. This clearly emphasizes the importance of examining this particular stream in relation to the others flowing in the Petra–Molyvos beach, making it a focal point of the analysis conducted in the present study. Specifically, the Petra stream extends about 6.0 km, while serving as a drainage system for an 8.0 km^2 area (the Petra basin, Figure 1b). In Figure 1c, the topographic and hydrological features of the Petra basin, together with the part of the stream included in the flood risk assessment, which will henceforth be referred to as the "Flood Assessment Area", are depicted.

In Lesvos, the geology is characterized by Miocene volcanic rocks that deposit above an Alpine basement, which consists of a Jurassic ophiolitic sequence overlying Paleozoic crystalline limestones and schists [32]. Three main geological units are detected in the island: (a) an autochthonous series of pre-alpine and alpine formations; (b) an allochthonous series of alpine volcano–sedimentary formations and ophiolitic rocks; and (c) post-alpine formations [32]. Volcanic rocks are predominant in the study area, as shown in Figures 2a and 3a. More specifically, along the coastline and the watershed, the main geological formations include alluvial plains (Q.al), dyke (Ng.d), upper lava unit (Ng.ul), and lower lava group (Ng.ll2) (Figures 2a and 3a) [33,34]. From a geomorphological point of view, the Petra–Molyvos coastline is characterized by rocky medium to high cliffs, and small seawalls, together with coastal and fluvial landforms (Figure 2a) [35,36].

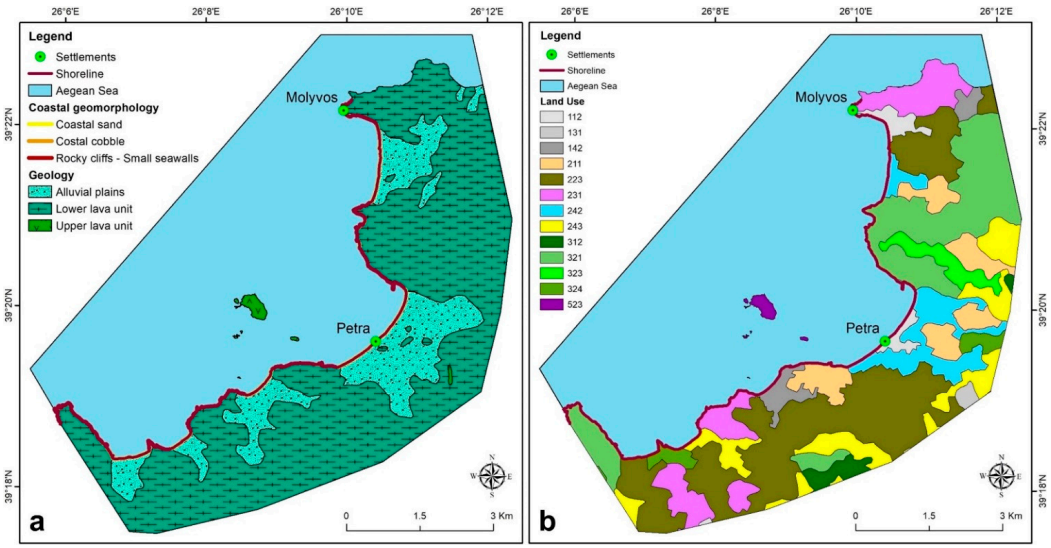


Figure 2. (**a**) The geomorphology of the coast under study, along with the geological formations identified in the region, and (**b**) the types of land use observed throughout the broader area, referring to the year 2018 (112—discontinuous urban fabric, 131—mineral extraction sites, 142—sport and leisure facilities, 211—non-irrigated arable land, 223—olive groves, 231—pastures, 242—composite culture systems, 243—land principally occupied by agriculture, 312—coniferous forest, 321—natural grassland, 323—sclerophyllous vegetation, 324—transitional woodland/shrub, 523—sea and ocean).

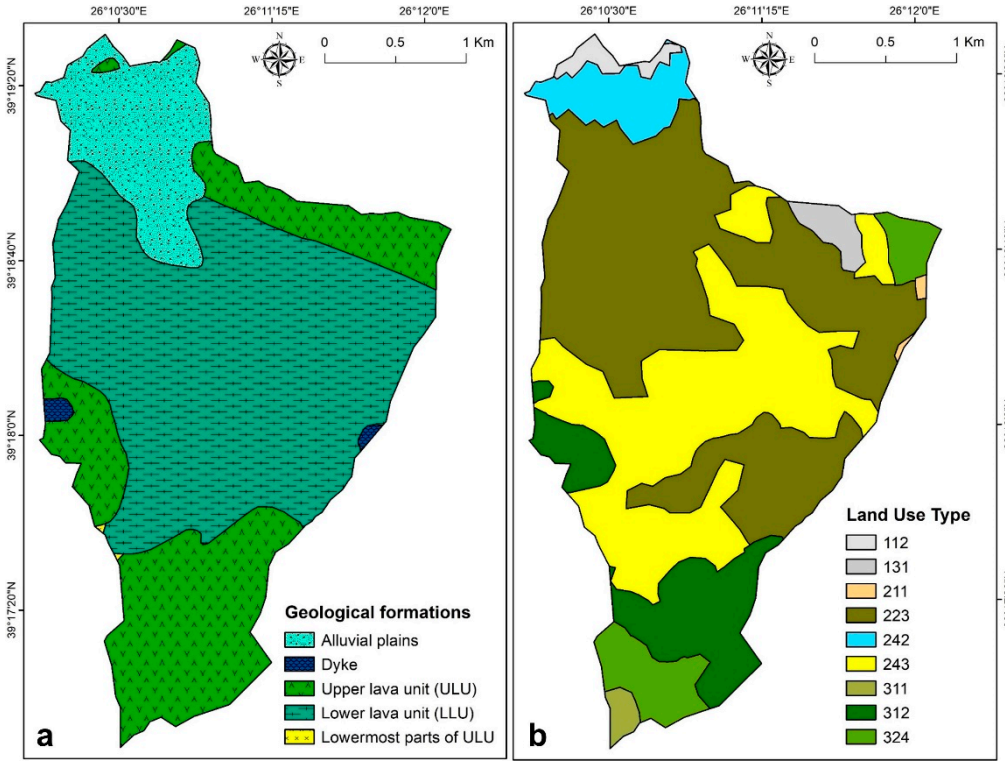


Figure 3. (**a**) The geological background of the Petra basin, and (**b**) the types of land use within the Petra basin, referring to the year 2018 (112—discontinuous urban fabric, 131—mineral extraction sites, 211—non-irrigated arable land, 223—olive groves, 242—composite culture systems, 243—land principally occupied by agriculture, 311—broad-leaved forest, 312—coniferous forest, 324—transitional woodland/shrub).

Concluding the study area description, the various land use types observed in the broader area surrounding the coastline, as well as within the Petra basin for the year 2018, are displayed in Figures 2b and 3b, respectively. As shown, the primary land cover comprises olive groves (code 223) and agricultural land (code 243), followed by either natural grassland (code 321) (Figure 2b) or forests (codes 311 and 312) (Figure 3b) [37,38].

2.2. Data Collection

For the needs of the present study, data related to both marine (i.e., sea level, waves) and hydrological (i.e., precipitation) parameters, as well as to the geomorphology of both the coastal area and the watershed, are required. Table 1 provides a brief description of the data used, also involving their sources, while outlining the specific processes for which the various data are needed. In addition to the data gathered from various sources, field measurements were also carried out specifically aimed at obtaining the necessary topographic data for the hydraulic simulations performed to produce water surface profiles and then convert them to flood inundation maps [39]. More specifically, nine cross-sections (XSs) along the downstream section of the Petra stream, in the interior of the "Flood Assessment Area" (Figure 1c), were measured using a TopCon Hipper VR GNSS receiver for field surveys. The measurements were taken from downstream to upstream, allowing for a comprehensive understanding of the stream's cross-section characteristics [39–41].

Table 1. The complete set of data gathered within the present study, including a brief description, their source, and the specific processes for which the various data are needed.

Data	Description	Process *	Source
Bathymetry	Raster file of the area of interest with a pixel size of 100 m × 100 m.	CV	European Marine Observation and Data Network (EMODnet) (europa.eu)
Relief	This parameter is defined as the average surface elevation—DEM raster file with a 27 m resolution.	CV, HC, HS, SY	Copernicus Land Monitoring Service
Surge Potential	The distance from the shore to the edge of the continental shelf, protected by a significant land mass—polylines created in QGIS 3.16.13.	CV	Shoreline/Coastline Databases | NCEI (noaa.gov)
Natural Habitats	Seagrass data exported from MARISCA project and converted into polylines in QGIS 3.16.13.	CV	Seagrass data by [42]
Geomorphology	Classification of physical characteristics including descriptions and ranks—polylines created in QGIS 3.16.13.	CV	European Marine Observation and Data Network (EMODnet) (europa.eu)
Climatic Forces	Wind–wave exposure model in MATLAB R2022b—hourly data at a height of 10 m (January 2017–December 2022).	CV	Meteoblue Monioudi, and Velegrakis [43]
Sea Level Rise	ESLs are considered the sum of the mean sea level, the astronomical tide, and the episodic coastal water level rise due to storm surges and wave setups (present and future scenarios—RCPS 4.5 and RCPs 8.5).	CV	Global probabilistic projections of extreme sea levels show intensification of coastal flood hazard | Nature Communications [44]
Landmass	Outline of the coastal region—modified polygon in QGIS 3.16.13.	CV	DIVA-GIS
Land Use	Modified polygon in QGIS 3.16.13 (CLC Version 2018).	CV, HC, HS, SY	Copernicus Land Monitoring Service
Precipitation	Statistical analysis of daily rainfall data (July 2009–October 2022).	SY, HC	Meteo.gr
Geology	Modified polygon in ArcGIS 10.2.2.	CV, SY, HC	University of the Aegean—Department of Geography Cartography & Geoinformatics Laboratory

Table 1. *Cont.*

Data	Description	Process *	Source
Work Field	Use of the Topcon Hiper VR GNSS receiver for the collection of surface elevation data. (TopCon Way, State of California, CA, USA)	HS	University of the Aegean—Department of Marine Sciences Coastal Morphodynamics & Management & Marine Geology
Satellite Images	Use of historical data from the years 2003 and 2024 to examine changes in the evolution of both the coastal zone and the river mouth.	CWC	Google Earth

* CV = coastal vulnerability, SY = sediment yield, HC = hydrological calculations, HS = hydraulic simulations, CWC = coastal–watershed continuum.

2.3. General Methodological Framework

The methodological framework developed in this study aims to investigate and analyze the intricate interrelationships among the diverse components of coastal–watershed systems, including coastal vulnerability, sediment transport, and flood risk. A general overview of the proposed methodology is depicted in Figure 4, while its various parts are briefly described in the following: **Coastal Vulnerability Assessment—M1** (Section 2.3.1): assessing coastal vulnerability to erosion is crucial for identifying areas at risk due to various factors, providing valuable information for protecting both human infrastructure and ecosystems, and promoting the sustainability and resilience of coastal regions. **Sediment Yield Assessment—M2** (Section 2.3.2): estimating sediment transport from the watershed to river channels is vital for understanding catchment erosion, as well as for assessing sediment supply to the nearby coastal zone. **Flood Risk Assessment—M3** (Section 2.3.3): understanding river flood processes is essential for assessing the potential severity of fluvial flood risks, and for evaluating sediment retention in flood-affected areas.

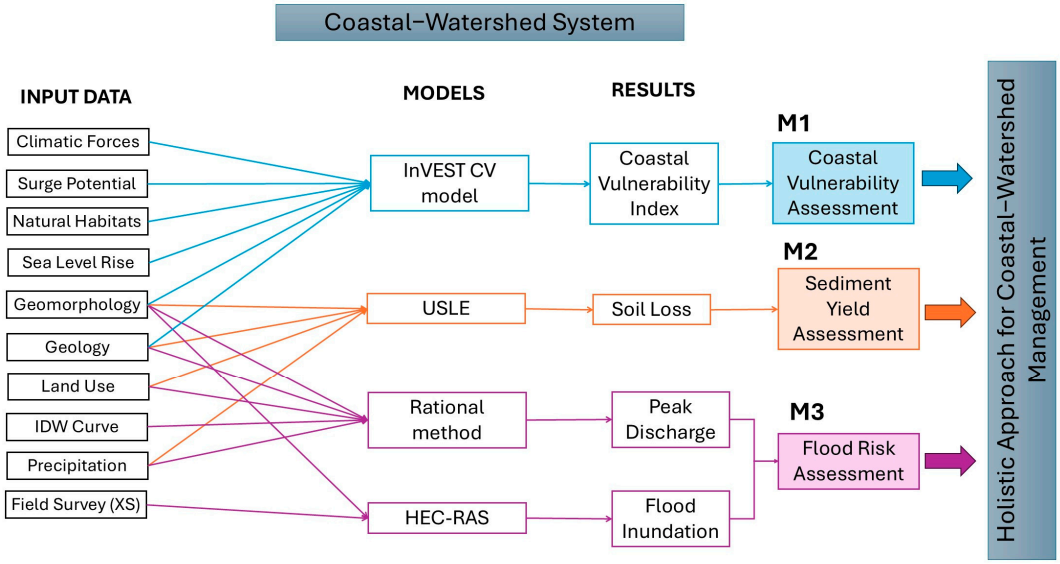


Figure 4. Graphical representation of the methodological framework developed in the present study to investigate the interconnection among coastal vulnerability, sediment transport, and river flood risk.

2.3.1. Coastal Vulnerability Assessment

The coastal vulnerability assessment was carried out using the Integrated Valuation of Ecosystem Services and Tradeoffs tool (InVEST) version 3.10 (Coastal Vulnerability Model—InVEST®), for the area of Petra–Molyvos, north Lesvos. The InVEST Coastal Vulnerability model is a fundamental tool for the comprehensive assessment of coastal vulnerability in different environmental conditions, covering areas with coral reefs, mangroves, urban shorelines, and remote, less-developed coastal regions. The importance of accuracy decreases with spatial scale expansion, especially for variables like geomorphology and bathymetry. Despite this limitation, the model remains a valuable and comprehensive tool that assists users in the precise evaluation of current coastal vulnerability, leading to making decisions for new strategies for the confrontation of erosion and integrated coastal management in the area of interest [13].

The exposure index was ranked for each point along the coastline with a user-defined interval. The exposure index indicates the comparative vulnerability of distinct coastal segments to erosion resulting, i.e., from surge storms, and sea level rise within the designated area of concern [4,13]. The model is designed to calculate the coastal vulnerability exposure index (CVI) by evaluating seven bio-geophysicals: wind and wave exposure, surge potential, sea level rise, geomorphology, natural habitats, and relief [10]. The rank of vulnerability exposure varies from very low vulnerability (rank = 1) to very high vulnerability (rank = 5). The primary data of the study area (Table 1) were processed using the mapping software QGIS 3.16.13.

The vulnerability index assesses coastal erosion, in which the high exposure of CVI indicates high vulnerability, and the coastal zone is easily eroded due to exposure to storms and waves. On the other hand, a low index exposure indicates a low vulnerability, and the coastal area is less affected by natural hazards. The geomorphology and natural habitats have been classified according to the model user guide InVEST (Table 2—Coastal Vulnerability Model—InVEST®). The formula of the coastal vulnerability index (CVI) for each shoreline point is the geometric mean of all variable ranks (Equation (1)). Consequently, the final product produced by the model is the total degree of vulnerability of all seven parameters studied, represented as points on the map of the study area [4,13].

$$CVI = \left(R_{geomorphology}\ R_{relief} R_{wave} R_{wind} R_{habitats} R_{surge} R_{SLR}\right)^{1/7} \quad (1)$$

Table 2. Bio-geophysical parameters and their respective classification ranges at each shoreline point.

Variables/Rank	Very Low	Low	Moderate	High	Very High
Geomorphology	Rocky, high cliffs, seawalls	Medium cliff, bulkheads, small seawalls	Low cliff, alluvial plain, rip-rap	Cobble beach, lagoon, bluff	Barrier beach, sandy beach, mudflat
Natural Habitats	Coral reef, mangrove, high saltmarsh	High dune, low marsh	Low dune, scrubland	Seagrass, kelp	No habitats
Relief, Wind and Wave Exposure, Surge Potential	0 to 20%	21 to 40%	41 to 60%	61 to 80%	81 to 100%
Seal Level Rise	0–1.0 m	1.1–1.30 m	1.31–1.60 m	1.61–1.90 m	>1.91 m

The estimation of the importance of wind exposure and wind-generated waves is required. It is presumed that the wave conditions under specific wind forcing and duration can be described by specific wave energy density spectra, such as the JONSWAP Spectrum, and are better suited in cases with fetch restrictions. The model requires wind statistics for at least 5 years and the average wind speed in each of the 16 equiangular sectors, where wind speeds in the 90th percentile or greater were observed near the segment of interest,

to compute the Relative Exposure Index (REI) or the highest 10% values and associated directions (Figure 5). For the wave computation from wind and fetch characteristics, the model requires the average of the wind speeds that are greater than or equal to the 90th percentile observed in each of the 16 equiangular sectors [43].

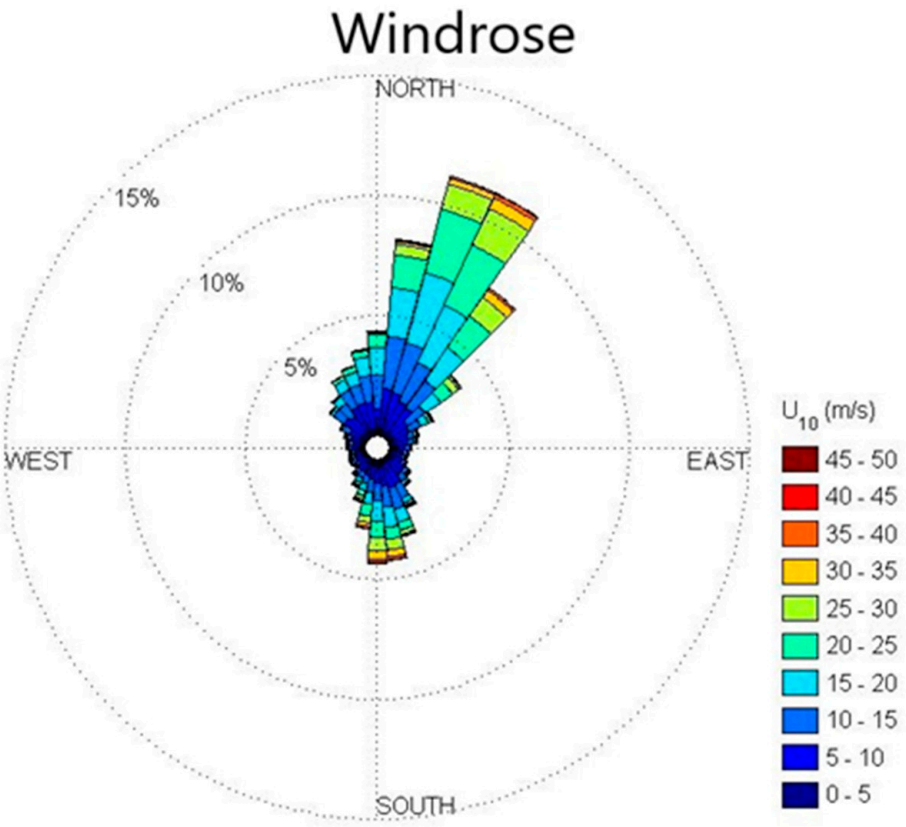


Figure 5. A Windrose depicting the primary wind directions in Petra–Molyvos and used to estimate wind exposure in the study area, during the period from 2017 to 2022.

In wind analysis, the JONSWAP–Pierson–Moskowitz (JONSWAP-P-M) method is used, which estimates the open sea significant wave height (Hs) and the wave period (Tp) of maximum energy density, based on the controlled wind speed U_A (Equation (2)), the effective fetch (Feff), (Equation (3)), and the wind duration (tD) [45,46].

$$U_A = 0.71\ (U_{10})^{1.23} \quad (2)$$

where U_A is the controlled wind speed, and U_{10} is the wind speed at 10 m above the sea surface (Figure 5). The wind–sea surface energy transfer increases with the time of wind flow above the sea surface–wind duration (tD).

$$F_{eff} = \frac{\sum_i F_i (cosa_i)^2}{\sum_i cosa_i} \quad (3)$$

where F_{eff} describes the radius direction 5° on either side of the wind direction, F_i is the linear fetch of the direction, and a_i is the angle of radius i with the wind direction.

For the computation of wind and wave exposure, a point shapefile was created with the following columns [13]:

- *REI_VX*: variable of wind speed that estimates the REI of each shoreline segment.
- *REI_PCTX*: corresponding to the proportion of the highest 10% wind speeds, which are centered on the main sector direction X.
- $W_{av}P\_X$: wave exposure variable for sites that are directly exposed to the open ocean.

- $W_{av}PCT\_X$: in combination with WavP_X, the wave exposure was calculated for locations that face the open ocean and represents the proportion of the highest 10% wave power values centered around the primary direction X.
- $V_{10}PCT\_X$: This parameter is utilized for wave power estimation based on fetch. It represents the mean of the highest 10% wind speeds centered around the primary direction X.

The projections of Extreme Sea Levels (ESLs) for the 21st century under the IPCC representative concentration pathway scenarios RCP4.5 and RCP8.5 were obtained from the global database (with a coastal grid resolution of 25 km) presented in the work of Vousdoukas et al. [44]. In this work, ESLs at the coast are a combination of i) the relative sea level rise (RSLR) due to eustatic changes, ii) the astronomical tide (η_{tide}), and iii) the episodic coastal water levels (η_{CE}) due to storm surges and wave setups. The ESLs occurring once in 10, 50, and 100 years, as calculated for the baseline year—2000—and the reference years 2050 and 2100, have been extracted from the database (Table 3) and were considered as an optional input parameter in the Invest model (Table 2).

Table 3. Ranges of extreme sea level rise (ESLs) for the three return periods (10, 50, and 100 years) and their components correspond to the wave conditions along the Petra–Molyvos coastline for different dates and under the climate scenarios.

	Tr	**Baseline**	**RCP 4.5**		**RCP 8.5**	
		2000	**2050**	**2100**	**2050**	**2100**
RSLR (m)	-	0	0.19	0.51	0.22	0.76
η_{Tide} (m)	-	0.12–0.13	0.12	0.12–0.13	0.12	0.12–0.13
η_{CE} (m)	10	1.19	1.17	1.16	1.17	1.12
	50	1.35	1.34	1.33	1.34	1.28
	100	1.42	1.4	1.39	1.4	1.34
ESL (m)	10	1.31–1.32	1.48–1.49	1.80–1.81	1.51–1.52	2.01
	50	1.48	1.65–1.66	1.96–1.97	1.68–1.69	2.16–2.17
	100	1.54–1.55	1.72	2.03–2.04	1.74–175	2.22–2.23

The intriguing aspect of the SLR parameter is usually variation over time between scenarios, rather than its spatial variation within a scenario. Unlike most other variables and the model, which are tailored to exhibit relative differences in spatial terms, the SLR parameter exhibits changes that vary both by region and across different scenarios. Due to the specificity of the SLR parameter, the user is responsible for calculating and classifying the input data. For the Petra–Molyvos study area, the data were classified based on the scale provided in Table 2.

2.3.2. Sediment Yield Assessment

In the present study, the Universal Soil Loss Equation (USLE) method was applied to estimate the soil loss in the Petra basin, while the sediment delivery ratio (SDR) module was used to calculate the sediment release at its outlet. The USLE is a mathematical model developed in order to estimate the amount of soil erosion by water, and it is widely used in soil conservation planning and land management practices [47–49]. The model considers several factors affecting soil erosion, including rainfall patterns, soil type, topography, land use types, and management practices [49–51]. The USLE equation (Equation (4)) in its original form, which is used to calculate the annual average rate of soil loss, is expressed as follows:

$$A = R \times K \times LS \times C \times P \quad (4)$$

where A is the soil loss per unit of area (t ha^{-1} yr^{-1}), R is the rainfall erosivity factor (MJ mm ha^{-1} h^{-1} yr^{-1}), K is the soil erodibility factor (t h MJ^{-1} mm^{-1}), LS is the topographic factor involving the slope length (L) and steepness (S), C is the cover and management factor, and P is the support practice factor.

Rainfall Erosivity Factor R

The rainfall erosivity factor (R) quantifies the intensity and frequency of rainfall events that contribute to soil erosion [52]. Given the inadequate availability of detailed rainfall data, it is usually estimated using mean monthly or even mean annual rainfall data, through the application of alternative equations specifically designed for this purpose [36,51,53]. In the current study, the R-factor was calculated by applying an equation produced by Vachaviolos [54] (Equation (5)), through which a linear relationship between the erosivity factor and the annual precipitation was established (R^2 = 0.8107). This certain equation was formed through correlation analysis of the studied variables after calculating the R-factor using detailed rainfall data obtained from the Mytilene airport rain gauge and analyzing 5 min rainfall heights for a range of significant events that occurred from 1988 to 2008. The rationale for using this equation to compute the R-factor lies in the fact that it was derived through detailed calculations based on data obtained from a meteorological station located in close proximity to the study area (about 40 km), exhibiting a similar climatic regime to that of the Petra basin.

$$R = 3.41P_{AN} - 382.4 \quad (5)$$

where R is the rainfall erosivity factor (MJ mm ha^{-1} h^{-1} yr^{-1}) and P_{AN} is the annual rainfall (mm yr^{-1}).

Data on rainfall between 2011 and 2022, obtained from a meteorological station within the Petra basin, were used to calculate the mean annual rainfall, and then to compute the mean R-factor corresponding to the examined time period. Through this process, the R-factor was determined to be 1495 MJ mm ha^{-1} h^{-1} yr^{-1}, which was assumed to be uniform across the entire basin.

Soil Erodibility Factor K

The soil erodibility factor (K) is a sensitive parameter, which is significantly associated with soil structure and characteristics, representing the susceptibility of soil to erosion [47,48,55]. In the present analysis, due to the lack of detailed data related to soil texture and permeability, the calculation of the K-factor was based on the geological background of the study area. More specifically, for each geological formation present in the region (Figure 3b), the K value was determined (Table 4 and Figure 6a) by taking into consideration lists of empirical observations from the relevant literature sources [53,56–58].

Table 4. K-factor values according to the geological formations within the Petra basin.

ID	Geological Formations	K
Q.al	Alluvial plains (clay, sand, gravel, fluvial deposits)	0.030
Ng.d	Dyke	0.020
Ng.ul	Upper lava unit	0.022
Ng.II_2	Lower lava unit	0.020
Ng.ul_1	Lowermost parts of the upper lava unit	0.022

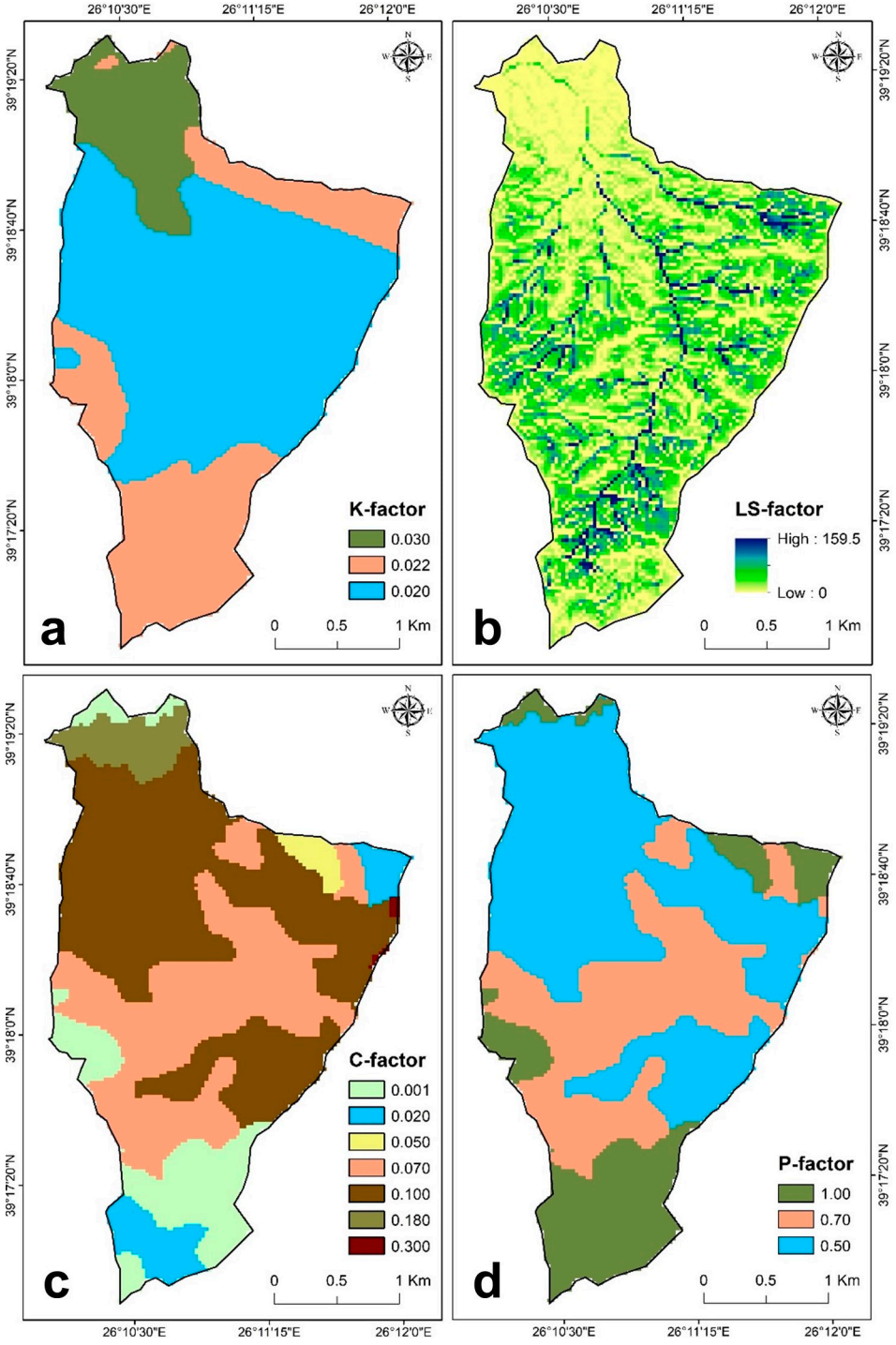


Figure 6. Map depiction of USLE factors for the Petra basin: (**a**) K-factor, (**b**) LS-factor, (**c**) C-factor, and (**d**) P-factor.

Topographic Factor LS

The topographic factor (LS), representing the combined effect of slope length (L) and slope steepness (S), corresponds to the ratio between the soil loss of a given slope length and steepness to the original USLE unit plot (L = 22.13 m and steepness 9%) [47,48]. In this study, the LS values were obtained by employing Equation (6), following the methodological

approach of Mitasova and Mitas [59], with the calculations performed in a GIS environment. The spatial distribution of the LS-factor is illustrated in Figure 6b.

$$LS = (m+1)\left(\frac{A_s}{22.13}\right)^m \left(\frac{sin\beta}{0.09}\right)^n \quad (6)$$

where m ranges from 0.40 to 0.60, m = 0.40 [59] in the present study, n ranges from 1.0 to 1.30, n = 1.1 [59] in this study, As is the specific catchment area representing the runoff upstream contributing area per unit width and calculated by applying the following raster function: "flow accumulation/cell size" (using ArcGIS), and β is the topographic slope in degrees.

Cover and Management Factor C

The cover and management factor (C) quantifies the counteractive impact of cropping and management practices on water-induced soil erosion and is actually associated with the land use types existing in the area of interest [53,60]. In the present study, the distribution of land use types in the year 2018 was considered (Figure 3b), in conjunction with empirical values acquired from the respective literature [52,53,60]. Table 5 displays the C value for each land use type detected in the Petra basin, while in Figure 6c, its spatial distribution is depicted.

Table 5. C- and P-factor values for each land use type within the Petra basin.

CLC Code	Land Cover	C	P
112	Discontinuous urban fabric	0.001	1.00
131	Mineral extraction sites	0.050	1.00
211	Non-irrigated—arable land	0.300	0.70
223	Olive groves	0.100	0.50
242	Composite culture systems	0.180	0.50
243	Land principally occupied by agriculture, with significant areas of natural vegetation	0.070	0.70
311	Broad-leaved forest	0.001	1.00
312	Coniferous forest	0.001	1.00
324	Transitional woodland shrub	0.020	1.00

Conservation Practices Factor P

The support practice factor (P) describes the effects of practices such as contouring, strip cropping, concave slopes, terraces, grass hedges, silt fences, and surface drainage systems, and serves as an indicator of the overall effectiveness of the practices in mitigating soil erosion [48,60]. In the case of implementing none of those conservation techniques, the P-factor is assigned a value of 1.0. In this study, the estimation of the P-factor, similar to the C-factor, relied on the land use types existing in the region (Figure 3b), while applying the same assumptions as Michas et al. [53] for a nearby basin as regards the implementation of soil conservation practices (Table 5 and Figure 6d).

The implementation of the USLE model was performed in a GIS environment. More specifically, for each parameter involved in the USLE (R, K, LS, C, and P), digital geospatial data layers were created in a raster grid format using the same grid as the DEM (27 m × 27 m). The final soil loss map was generated by overlaying the corresponding parameters maps and using Equation (4).

As far as the sediment yield is concerned, the SDR concept was used. The SDR is a metric that represents the ratio between the estimated sediment yield at a particular stream point and the total amount of upland soil erosion that occurs upstream of that point. Several

equations, mainly based on the topography and physiography of the area of interest, have been developed to calculate the SDR [47,48,53]; in the present study, Vanoni's formula [61] (Equation (7)), which has also been applied in a nearby basin [53], was used as follows:

$$SDR = 0.4724 \times A^{-0.125} \quad (7)$$

where SDR is the sediment delivery ratio and A is the catchment area (km^2).

2.3.3. Flood Risk Assessment

For assessing flood risk in the study area, both hydrological calculations to estimate peak discharge and hydraulic simulations to generate water surface profiles are required. The rational method was utilized for calculating the peak discharge required as input for the hydraulic simulations conducted for the selected "Flood Assessment Area". More specifically, peak discharge for three different return periods (5-year, 50-year, and 100-year) at junction J3 (Figure 7), which is located upstream of the "Flood Assessment Area", was computed, taking into consideration the tributaries contributing to the junction (SB2, SB3, SB4, SB5, SB6, and SB7). With regard to the hydraulic simulations, three different simulations were conducted, each one corresponding to a different return period, in order to calculate cross-section-specific flow characteristics and assess flood risk in the "Flood Assessment Area" (Figure 7). All simulations were performed under steady-state conditions (1D simulations) using the discharge flows of Junction J3, through the application of the Hydrologic Engineering Center's River Analysis System (HEC-RAS 5.0.6) software [62].

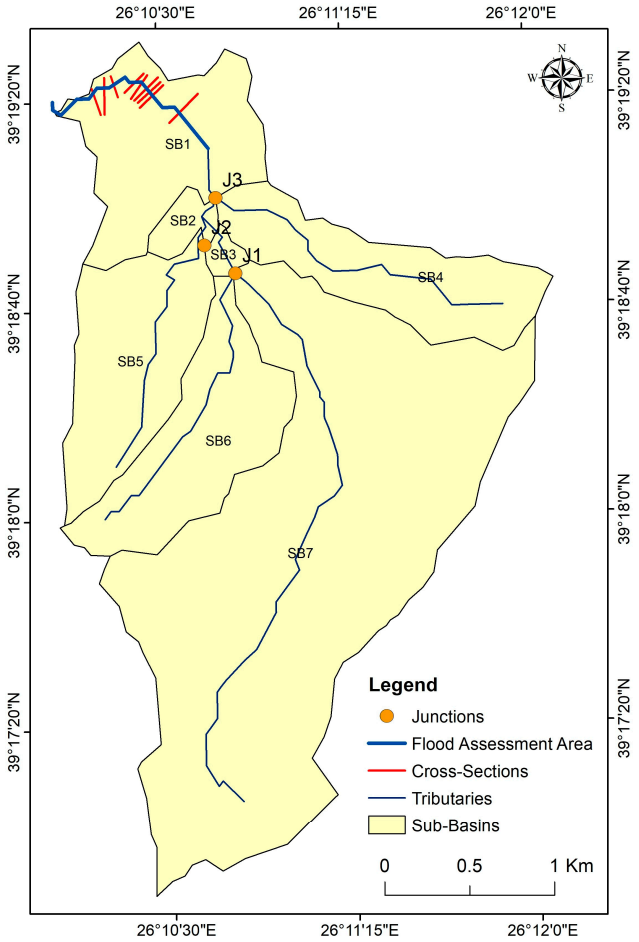


Figure 7. The seven sub-basins and the three junctions (J1–J3) of the study area, along with the main tributaries (SB1–SB7), the "Flood Assessment Area" and the nine cross-sections located in its interior and considered in the hydraulic simulations.

Rational Method

The rational method is one of the most well-known common hydrological design tools for determining peak discharges in small insular catchments, having been used by several researchers globally [63–67]. In Greece, in accordance with the national guidelines pertaining to stormwater projects (PD696/74), implementation of the rational method should be limited to drainage areas less than 10 km^2 [68,69], thus being appropriate for the Petra basin.

The rational formula is generally expressed by Equation (8):

$$Q = 0.278 \times i \times C \times A \quad (8)$$

where Q is the peak discharge ($m^3\ s^{-1}$), i is the rainfall intensity factor (mm hr^{-1}) over a critical period of storm time (typically taken as the time of concentration of the drainage area), C is the runoff coefficient (dimensionless), and A is the drainage area (km^2).

Determining both the rainfall intensity factor and the runoff coefficient constitutes a crucial step in the whole procedure [70–73]. Regarding the former, the rainfall intensity factor (i) was calculated based on an IDF (Intensity–Duration–Frequency) curve obtained from the River Basin Flood Risk Management Plan for the Water District of the Aegean Islands [74] and specifically formed based on rainfall data from the Kerami station, which is adjacent to the area of interest. The mathematical expression of the Kerami station IDF curve is defined as follows (Equation (9)):

$$i(d, T) = \frac{472.98\left(T^{0.093} - 0.734\right)}{\left(1 + \frac{t_c}{0.134}\right)^{0.741}} \quad (9)$$

where T is the return period (years) of the design storm and t_c is the time of concentration for the drainage area (hrs). For computing the time of concentration, Giandotti's formula was used. In Table 6, the geomorphological characteristics, together with the corresponding concentration times of each sub-basin, are presented. Based on these values, while taking into consideration the tributaries contributing to junction J3, the longest time of concentration was defined for the junction (SB7 → SB3 → SB2). Then, by applying Equation (9), the rainfall intensity factors corresponding to the longest concentration time for each return period were determined (Table 7).

Table 6. The geomorphological features of all sub-basins, together with the respective concentration times calculated using Giandotti's formula.

Sub-Basin	Area (km^2)	Mainstream Length (km)	Mean Sub. Elevation (m)	Outlet Elevation (m)	Mean Sub. Slope (%)	t_c (hrs)
Sub 1	0.91	1.55	13.86	6.00	5.41%	2.74
Sub 2	0.11	0.27	17.19	9.00	6.49%	0.74
Sub 3	0.05	0.30	17.88	12.00	8.02%	0.69
Sub 4	0.82	2.11	166.37	10.00	26.81%	0.68
Sub 5	0.89	1.75	121.76	13.00	24.40%	0.77
Sub 6	0.90	1.85	160.95	19.00	26.65%	0.69
Sub 7	4.37	4.35	261.64	21.00	29.72%	1.20

Table 7. The values of the parameters included in the rational method, along with the peak discharge values for the three different time periods at Junction J3.

Junction	T (years)	t_c (hrs)	i (mm h^{-1})	Area (km^2)	C	Q (m^3 s^{-1})
J3	5	2.63	21.46	7.14	0.58	24.6
	50		35.38		0.69	48.7
	100		40.19		0.72	57.7

As far as the runoff coefficient is concerned, it was determined following a literature-based procedure [68], while considering important catchment characteristics that affect runoff, such as topographical, geological, and land use information. Moreover, the proportionality technique was used to calculate a "weighted" runoff coefficient for each sub-basin [68,73], while three distinct runoff coefficients, each one corresponding to a different return period, were computed using certain conversion factors. Based on the runoff coefficients of each sub-basin, while taking into consideration the sub-basins contributing to junction J3, a new "weighted" C value for the junction was defined for each return period. Finally, after calculating both the rainfall intensity factors and the runoff coefficients, and applying Equation (8), the peak discharge values at junction J3 for each return period were determined (Table 7).

Hydraulic Simulation

As a prerequisite step for conducting the hydraulic simulations, detailed geometric and topographic data are required to define both the river geometry parameters (i.e., stream centerlines, riverbank lines, flow path lines, and XS cut lines) and the flood area physical characteristics [39,40,67,75]. In order to achieve this, the DEM obtained for the study area was combined with the field measurements in an effort to accurately capture the geometry of the main channel.

More specifically, at the first stage, the DEM was converted into a terrain TIN (Triangular Irregular Network) using the conversion toolbox provided in ArcGIS. Then, the HEC-Geo RAS tool, which is an integrated extension of ArcGIS, was utilized to generate the topography of the "Flood Assessment Area" and extract the necessary river geometry parameters. Next, the extracted data were imported in HEC-RAS, where XS cut lines were properly delineated and riverbanks were defined based on the field measurements, i.e., the measured river cross-sections. Through this process, an attempt to represent the geometry of the river's main channel as accurately as possible was made to compensate for the lack of a detailed DEM with a high spatial resolution. In Figure 7, the location of the nine river cross-sections considered in the hydraulic simulations is depicted together with the area where flood mapping is performed.

Another important step in hydraulic modeling is to properly define Manning's roughness coefficient n both for the main channel and the overbanks [26,32,76]. In the present study, a uniform value of 0.04 was used for the overbanks (both left and right overbank) based on the land use types of the "Flood Assessment Area" [68], while two different values were assigned to the main channel based on river irregularities and surface material. More specifically, a value of 0.02 was used for impermeable surfaces corresponding to the eight downstream cross-sections and a value of 0.04 for natural surfaces referring to the one upstream cross-section [61,74].

As a final step in the hydraulic modeling, the stream flow regime was selected, and the boundary conditions were specified. With regard to the former one, the sub-critical flow regime was chosen for integrating the type of flow regime in the examined reach, while concerning the latter one, normal depth was used as a boundary condition. According to this boundary condition type, the energy grade line slope values are assumed to be equal to the riverbed slope values [32,77], thus leading to assigning a specific value of 0.0045 at the downstream end of the examined reach, based on the average topographic slope of the reach. At this point, it should also be noted that since the present study aims to demonstrate

a generic methodology applicable to the proper and effective management of coastal zones in tourist destinations, rather than focusing on a specific case, no calibration and validation of hydraulic simulations in terms of predicted flood patterns were conducted.

3. Results

Maps and statistics were developed through the application of the Integrated Risk Assessment Framework, and they are presented in the following paragraphs, highlighting key indicators that drive coastal vulnerability and flood risk.

3.1. Coastal Vulnerability Assessment

Figure 8 illustrates the vulnerability values for each parameter in the shoreline of Petra–Molyvos, as determined by the InVEST model. The northern part of the study area, with its relatively low elevation, exhibits high vulnerability, whereas the southern and central portions, with their higher elevation, show very low vulnerability (Figure 8a—R: Relief parameter). Figure 8a illustrates the vulnerability values for the surge potential parameter along the shoreline, showing that the majority of the coast is classified as very high vulnerability. Under the influence of wind (Figure 8a) and waves (Figure 8b), vulnerability values range from high to very high in the central part of the coastline, while sheltered areas exhibit low to very low vulnerability. The beach, composed primarily of Quaternary alluvial sediments and partially of pyroclastic deposits, shows very high vulnerability (Figure 8b). In contrast, areas with lower vulnerability are predominantly composed of basalt and andesite bedrock. According to Topouzelis et al. [42], seagrass is the most important habitat in the inshore area, even though it does not play a significant protective role for the coastline. Consequently, this parameter exhibits very high vulnerability along the entire coastal stretch (Figure 8b).

Figure 8c and Table 8 show coastal vulnerability estimates based on sea level rise. According to the CVI, by the baseline and 2050, 54% of the shoreline will experience moderate vulnerability, while 44% will face high vulnerability. By 2100, under the RCP 4.5 scenario, 51% of the shoreline is expected to have moderate vulnerability and 47% high vulnerability for a 10-year return period. Under the RCP 8.5 scenario for the same period, 52% of the coastline is projected to be highly vulnerable. The comparative analysis of climate scenarios reveals consistent CVI values, with moderate vulnerability at 54% and high vulnerability at 44% by 2050. For the 50- and 100-year return periods, the projections are 51% moderate and 47% high vulnerability by 2050, and by 2100, the shoreline is anticipated to be 52% highly vulnerable and 46% moderately vulnerable. Considering all seven variables (Figure 8c), the estimated coastal vulnerability indicates that the Petra area is highly vulnerable. The coastal zone from Petra to Molyvos, including the Petra stream, generally exhibits moderate to high vulnerability. There are also a few small sections along the coastline with low vulnerability.

Table 8. Coastal Vulnerability Index estimation for both scenarios RCP4.5 and RCP8.5, which present the identical CVI of each return period (10, 50, and 100 years).

Return Period	RCP 4.5					RCP 8.5				
	Very Low	Low	Moderate	High	Very High	Very Low	Low	Moderate	High	Very High
Baseline T10	0.0%	2%	54%	44%	0.0%	0.0%	2%	54%	44%	0.0%
2050 T10	0.0%	2%	54%	44%	0.0%	0.0%	2%	54%	44%	0.0%
2100 T10	0.0%	1%	51%	47%	0.6%	0.0%	1%	46%	52%	0.6%
Baseline T50	0.0%	2%	54%	44%	0.0%	0.0%	2%	54%	44%	0.0%
2050 T50	0.0%	1%	51%	47%	0.6%	0.0%	1%	51%	47%	0.6%
2100 T50	0.0%	1%	46%	52%	0.6%	0.0%	1%	46%	52%	0.6%
Baseline T100	0.0%	2%	54%	44%	0.0%	0.0%	2%	56%	44%	0.0%
2050 T100	0.0%	1%	51%	47%	0.6%	0.0%	1%	51%	47%	0.6%
2100 T100	0.0%	1%	46%	52%	0.6%	0.0%	1%	46%	52%	0.6%

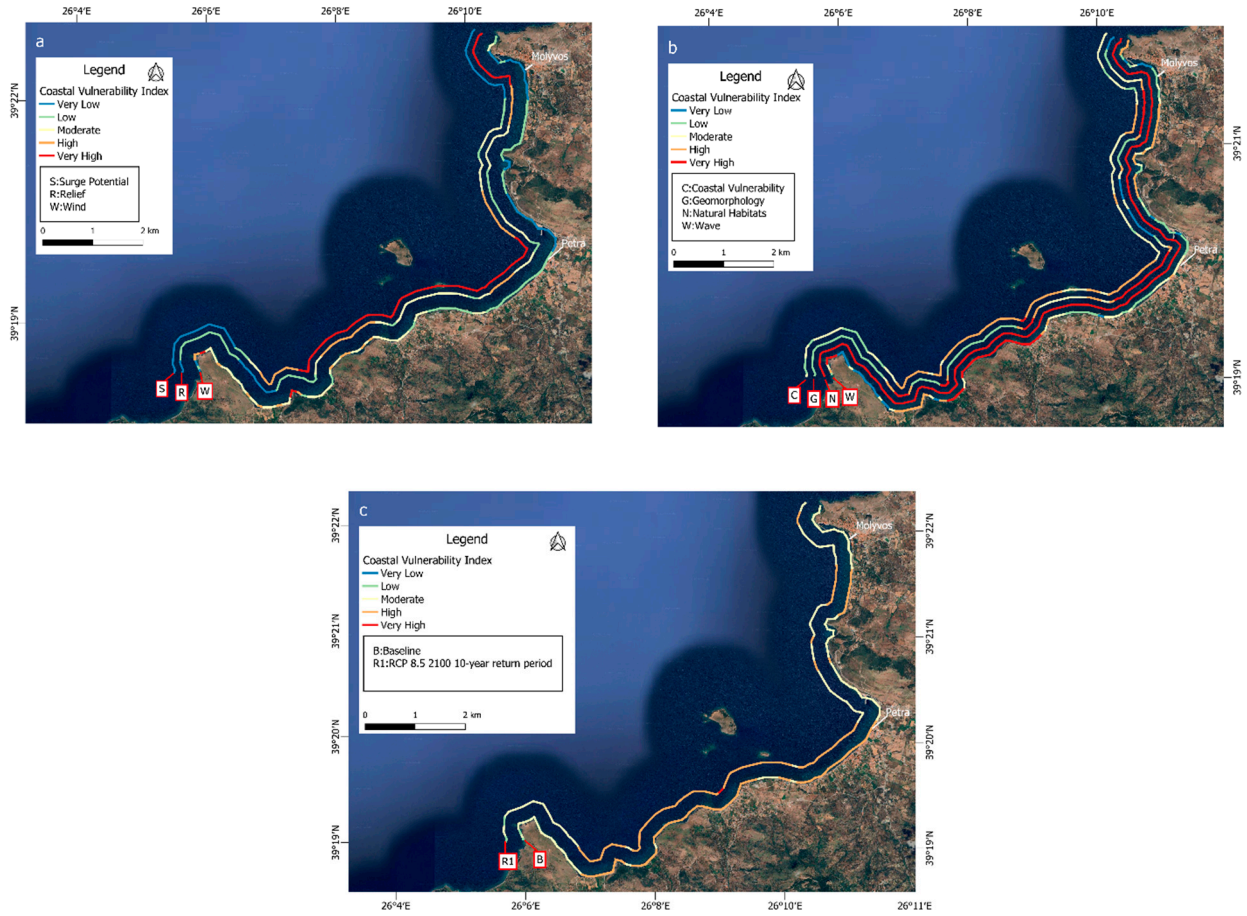


Figure 8. (**a**) The ranking evaluation of the first three parameters, i.e., Relief, Surge Potential, and Wind, of the coastal exposure index, (**b**) the ranking evaluation of the remaining parameters, i.e., Geomorphology, Habitats, Wave, alongside the Coastal Vulnerability estimated by the INVEST model considering all six parameters, and (**c**) Coastal Vulnerability also considering Sea Level Rise over a 10-year return period for the projected scenario RCP 8.5, compared to the previously estimated baseline scenario.

3.2. Sediment Yield Assessment

By applying the USLE method, the soil loss raster was generated, each pixel of which contains the annual soil loss value (t ha^{-1} yr^{-1}) based on the local parameters of this certain pixel. In Figure 9, the annual soil loss rate for the Petra basin is depicted considering five classes, each of which corresponds to a specific soil erosion level, defined as follows: (i) very low (0–5 t ha^{-1} yr^{-1}); (ii) low (5–15 t ha^{-1} yr^{-1}); (iii) moderate (15–30 t ha^{-1} yr^{-1}); (iv) high (30–50 t ha^{-1} yr^{-1}); and (v) very high (>50 t ha^{-1} yr^{-1}). The resulting map reveals a prominent pattern, where areas along the drainage network, characterized by high LS values (Figure 6b), exhibit significantly elevated soil erosion levels. Conversely, areas occupied by forest lands in the north parts of the region, as well as predominantly flat areas in the south (Figure 6c), demonstrate notably low soil erosion values. Furthermore, based on the analysis of the class area results, it is evident that a major part of the Petra basin (77.9%) falls within the categories of very low to low soil erosion classes, while high to very high soil erosion classes only encompass a mere 7.5% of the region.

Finally, Table 9 presents the mean and total annual soil loss for the Petra basin, as well as the mean and total annual sediment yield deposited at the basin's outlet. Sediment yield is of particular importance because it is directly related to the quantity of sediment that is transported and accumulated at the beach. In this context, it is worth mentioning that the estimated value of the mean sediment yield is 358 t km^{-1} y^{-1}, which is in complete agreement with the findings of Michas et al. [53], who estimated a sediment yield of

352 t km^{-1} y^{-1} for a nearby basin using similar methods, i.e., the USLE method, while performing an analytical calculation of the R-factor, specifically based on a five-minute rainfall time step.

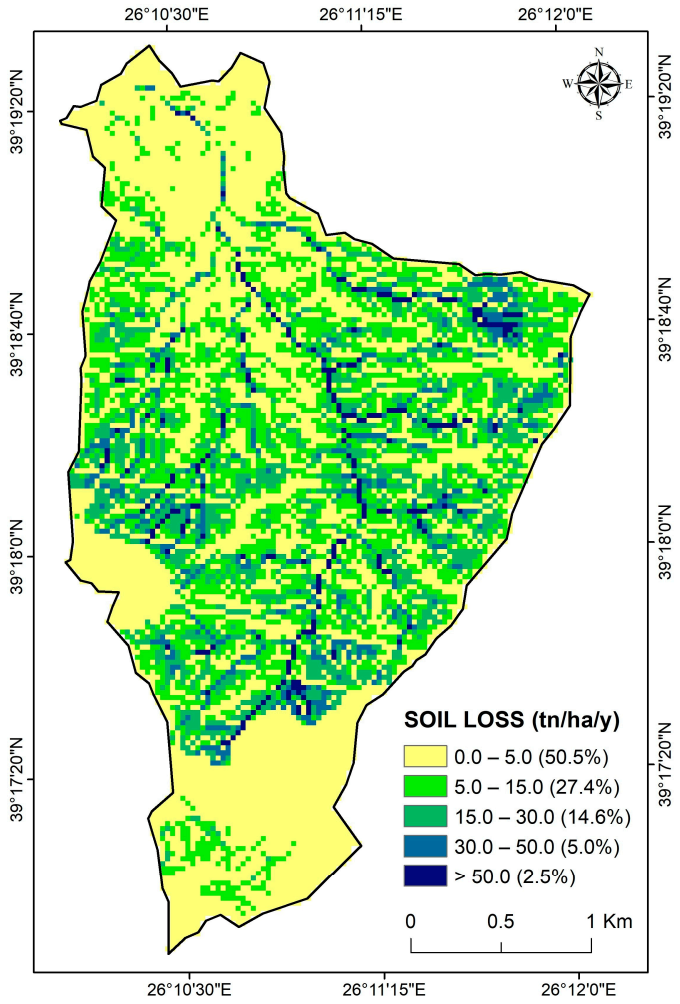


Figure 9. Soil loss distribution for the Petra basin (the areal percentage of each soil erosion class is given in parentheses).

Table 9. Soil loss and sediment yield at Petra basin.

	Parameters	Units	Values
Soil loss	Annual soil loss (per ha)	t ha^{-1} yr^{-1}	9.83
	Annual soil loss (per km^2)	t km^{-1} yr^{-1}	983
	Catchment area	km^2	8.0
	Total annual soil loss	t yr^{-1}	7860
Sediment yield	Reduction sediment yield factor (Vanoni)	-	0.364
	Annual sediment yield (per km^2)	t km^{-1} yr^{-1}	358
	Total annual sediment yield	t yr^{-1}	2860

3.3. Flood Risk Assessment

In Figure 10, the integrative water surface profile along the examined reach for all different flow discharges set at upstream (Junction J3) is depicted. As is apparent, water surface elevation generally decreases from upstream to downstream of the examined reach for all flow profiles, while, in all nine cross-sections, it rises as the flood events become more severe and the peak discharge increases, thus causing the examined reach to overflow its banks to a greater extent. During the 5-year return flood, three out of the nine cross-sections (XS-2, XS-7, and XS-8) experienced overflow (Figure 10), whereas the total number of overflown cross-sections increased to seven in both the 50-year and 100-year recurrence intervals. Only cross-sections XS-3 and XS-6 were found to have not experienced overflow during the different return periods. Moreover, cross-section XS-8 was found to be the more critical in terms of both flood extent and flow depth in relation to all other flow profiles.

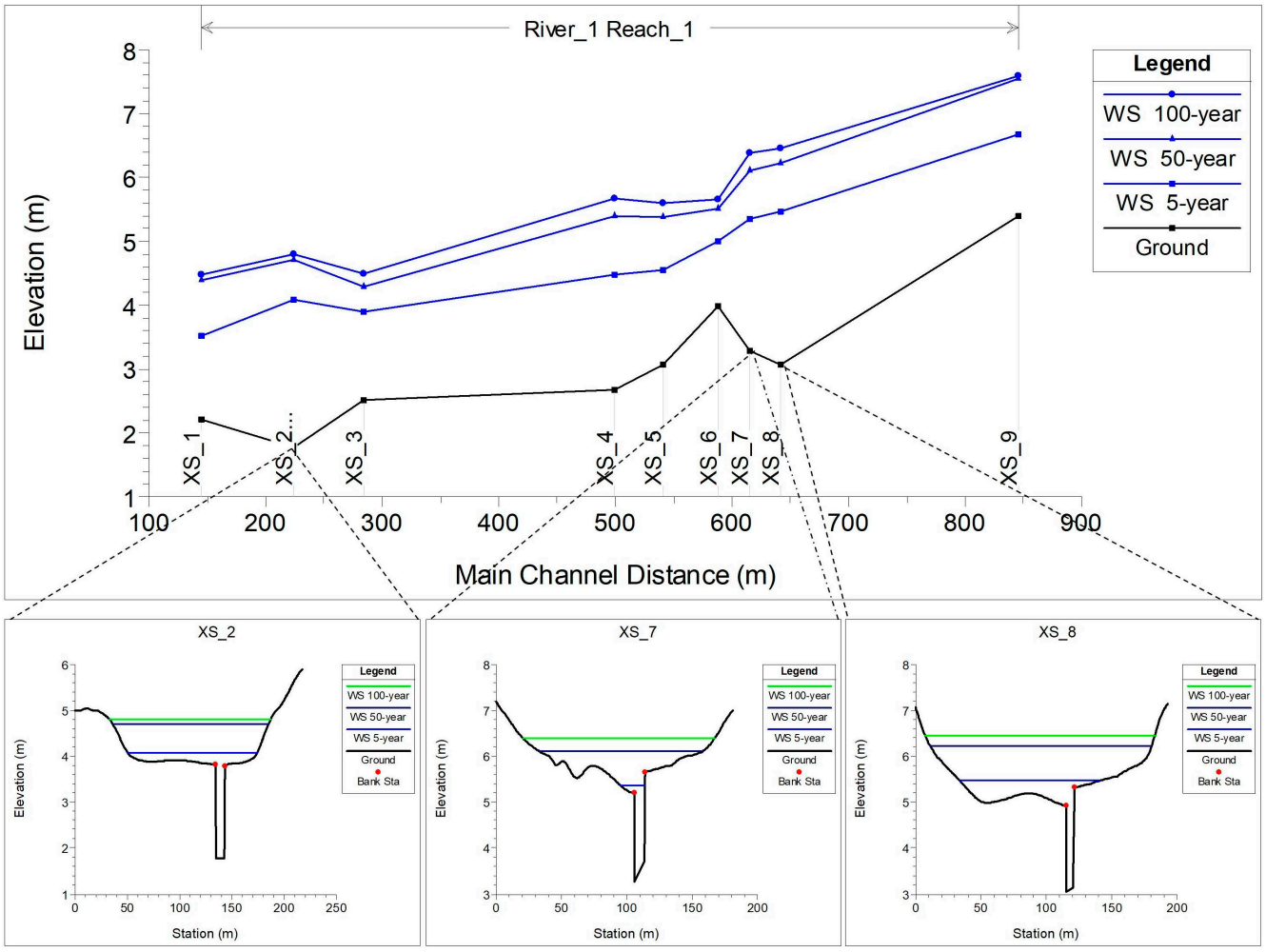


Figure 10. Integrative water surface profile along the examined reach within the "Flood Assessment Area", together with the plan view of water surface elevation at cross-sections XS-2, XS-7, and XS-8, for the three different flow profiles (5-year, 50-year, and 100-year return periods).

The same conclusions as above can also be extracted from the flood inundation maps of all flow profiles shown in Figure 11, and the flood characteristics presented in Table 10. As is obvious, the 50-year and 100-year recurrence interval peak floods inundated a relatively large part of the "Flood Assessment Area" (of the part included within the selected cross-sections, Figure 10), in comparison to the 5-year return flood, which mainly resulted in the inundation of areas adjacent to cross-sections XS-2, XS-7, and XS-8. Given these findings and the extensive flooding of the "Flood Assessment Area" during 50-year and 100-year

recurrence intervals, it can also be concluded that sediment retention can be relatively high, leading to reduced sediment accumulation at the basin's outlet.

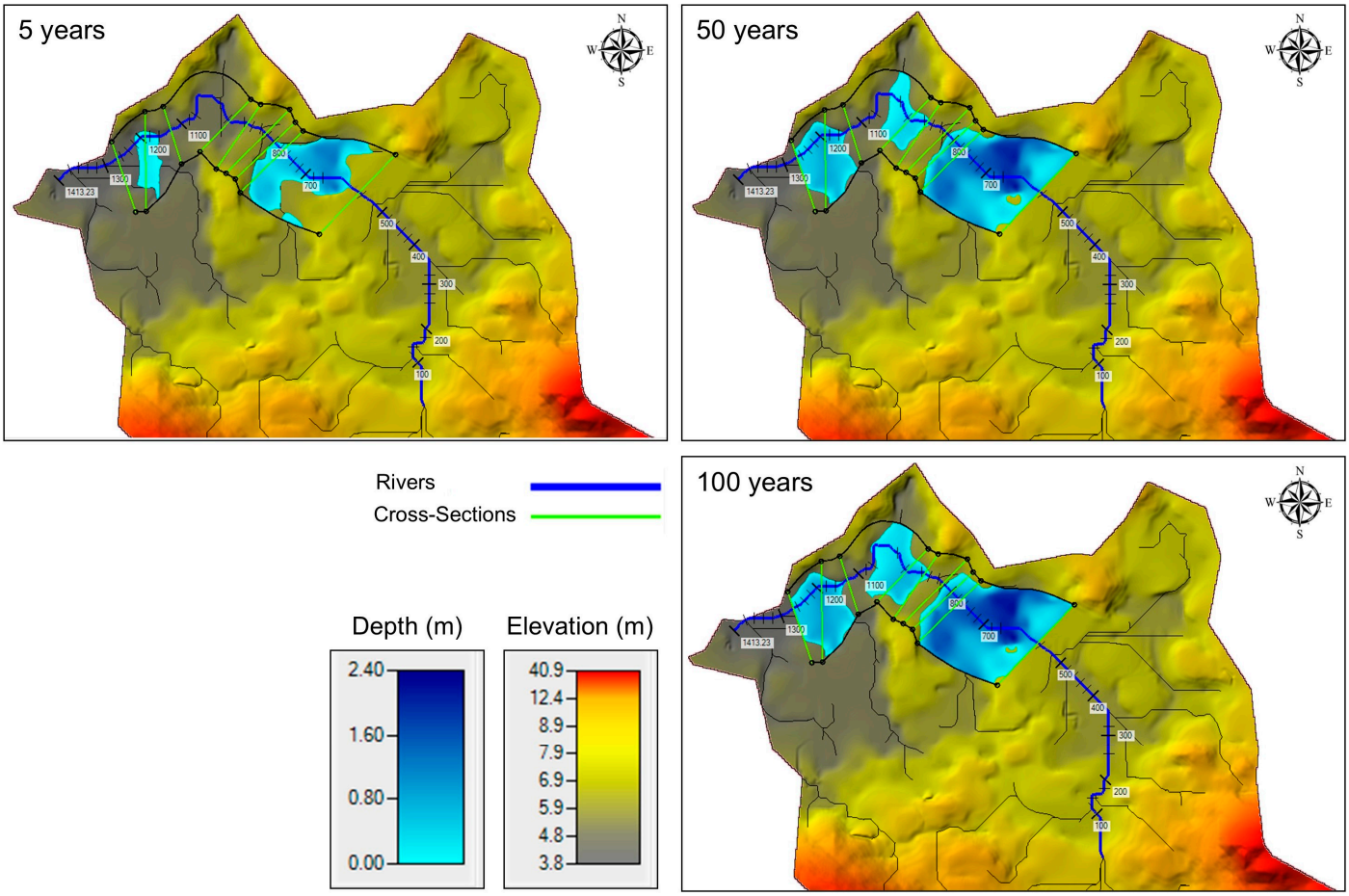


Figure 11. Flood inundation maps for the three different recurrence intervals (5-year, 50-year, and 100-year return periods).

Table 10. Flood characteristics for the three different recurrence intervals (5-year, 50-year, and 100-year return periods).

T (years)	Q (m^3 s^{-1})	Flood Inundation Area (km^2)	Percentages of Inundated Areas		Max. Flood Depth (m)
			Discontinuous Urban Fabric	Composite Culture Systems	
5	24.6	0.031	4.5%	95.5%	1.33
50	48.7	0.069	12.4%	87.6%	2.17
100	57.7	0.079	16.3%	83.7%	2.27

Next, by combining the produced inundation maps (Figure 11) with the land use map (Figure 3b), the type of land use affected by the examined flood events can be identified. As indicated in Figure 12, for all return periods, the majority of the inundated areas consist of agricultural lands, classified as composite culture systems (code 242), with the remaining areas belonging to the land use type referred to as discontinuous urban fabric (code 112). In Table 10, the percentages of the inundated areas for each of the aforementioned land use types are contained. According to this analysis, it can be inferred that, concerning the examined section of the Petra stream, agricultural lands exhibit a higher flood risk potential

compared to urban areas, particularly those situated upstream, adjacent to cross-sections XS-2, XS-7, and XS-8.

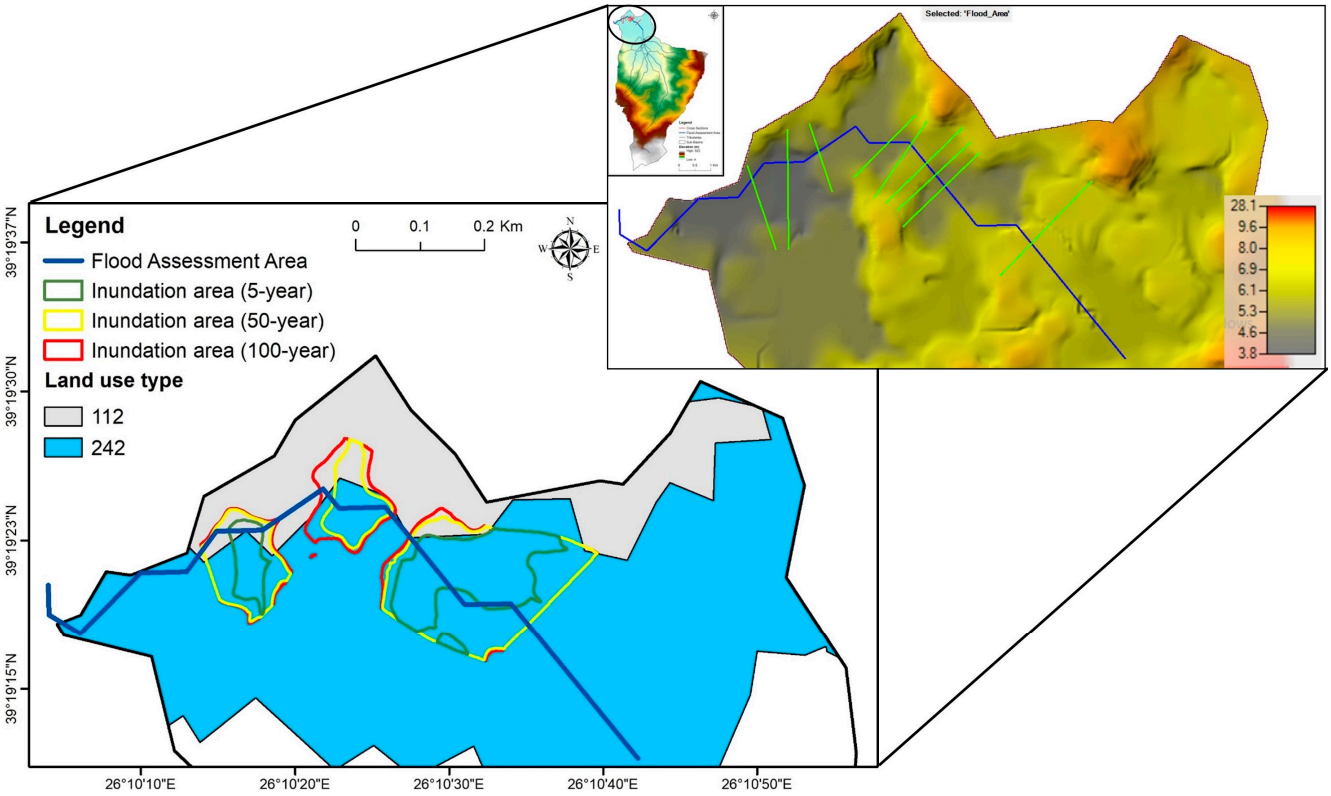


Figure 12. Inundated areas in each type of land use (112—discontinuous urban fabric, 242—composite culture systems) for the three different recurrence intervals (5-year, 50-year, and 100-year return periods).

4. Discussion

Three different components related to the coast–watershed system are considered and analyzed in the present study to develop a holistic approach toward integrated coastal area management. The interactions among coastal, land, and river settings are crucial for understanding sediment dynamics between the watershed and coast within a local region. The case study of the Petra–Molyvos coast presents a conceptual framework for understanding coastal–watershed interactions and their evolutionary changes. In this context, this study employed the InVEST Coastal Vulnerability model, USLE method, and the HEC-RAS model to develop a comprehensive framework applicable to small Mediterranean coastal areas.

4.1. Coastal Vulnerability Assessment

Based on the results of the coastal vulnerability assessment, the Petra–Molyvos shoreline faces moderate to high vulnerability to erosion (Figure 8). These observations, consistent with findings from other studies in the Mediterranean region [5,12], are primarily attributable to the natural characteristics of these areas, involving sea level rise changes, geomorphology, relief, surge potential, wind, waves, and natural habitats. Hence, combining these parameters indicates that coastal vulnerability will range from moderate to high (Figure 8b) along most parts of the shoreline being studied. Specifically, the CVI estimated that the adjacent coast to the river mouth is characterized by a very high vulnerability for 2100 with all return periods (10, 50, 100 years). Thus, marine dynamics contribute to coastal vulnerability to erosion, while coastal evolution is mainly affected by wind and wave actions.

However, it should be mentioned that severe historical records of events, such as flash floods or coastline changes due to sand/gravel removal, amendment, or transfer, are missing and therefore not accounted for in the CVI estimation. This highlights the challenges posed by data gaps and the difficulties in achieving measurement accuracy. While land use, coastal urban settings, and relief are easy to measure and adjust, access to specialized instruments is needed in order to accurately record bathymetry and wave dynamics, as well as marine biodiversity data. The shift to using open-access data (see Table 2) may hinder accurate estimations due to constraints such as large pixel size. Additionally, it is worthwhile to note that the socio-economic equilibrium of the area, which may be affected by environmental pressures, was not considered in the analysis conducted in this study. As a result, coastal transformations due to human activity were not directly taken into account in the CVI estimation [78]. Instead, they were addressed indirectly through the impacts of climate change (CC) scenarios. However, the uncertainty in CC projections significantly affects the estimation of the sea level rise (SLR) component of the CVI equation. Consequently, the CVI may provide spatial guidance for future research directions, rather than offering highly accurate modeling results.

4.2. Sediment Yield and Flood Risk Assessment

As regards the second part of the proposed methodology, the study area is characterized by low sediment deposition from the mainstream, while soil erosion within the basin is generally classified as very low to low. The sediment fluxes do not significantly support the Petra–Molyvos coast, while catchment erosion provides only a small contribution of terrestrial sediments to the Petra–Molyvos beach. Finally, according to the flood risk assessment outcomes, it turned out that, particularly in the cases of 50-year and 100-year recurrence intervals, severe flooding events may occur along the river's overbanks, leading to the flooding of the majority of the "Flood Assessment Area". Due to the concentration of water in flood-affected areas, sediment retention might be relatively high, further hindering its transport and accumulation at the basin's outlet.

Sediment accumulation in flood-inundated areas of intermittent flow streams is a crucial process in river geomorphological evolution. While it acts as a natural mechanism for sediment transport and deposition, human activities can significantly alter this process. Interventions in rivers can change flow regimes, leading to increased flooding phenomena and larger flood-affected areas, which, in turn, boost sediment retention and accumulation in the floodplains. However, the presence of floodplains is crucial for preventing excessive river erosion. Conservation practices for floodplains, such as restoring natural vegetation, maintaining river meandering patterns, and preserving seasonal river flow (e.g., avoiding overpumping for irrigation), can help mitigate excessive sedimentation and erosion, as well as reduce the rapid transfer of sediment to the coast [79].

4.3. Coast–Watershed System

Analyzing the coast–watershed system is crucial for understanding how these features are interconnected and how they influence coastal morphology and stability. Interactions between marine and terrestrial environments are dynamically linked through the continuous evolution of coastal morphology [11]. The limited sediment supply from the river and its adjacent coastal zone, combined with flow intermittency, reduces sediment availability from the terrestrial environment. This situation exacerbates coastal vulnerability to erosion phenomena induced by sea level rise and wind-generated waves. Additionally, human interventions, such as channelization and residential development, particularly at the river's mouth, increase flooding phenomena and expand flood-affected areas, thereby hindering sediment transport to the coast due to sediment accumulation on the floodplains. In this context, Figure 13a,b depict the mouth of the Petra river and the adjacent shoreline, highlighting areas that have experienced beach retreat over the past 21 years, while Figure 13c,d illustrate human activities and interventions in the river that alter the river regime and affect sediment transport.

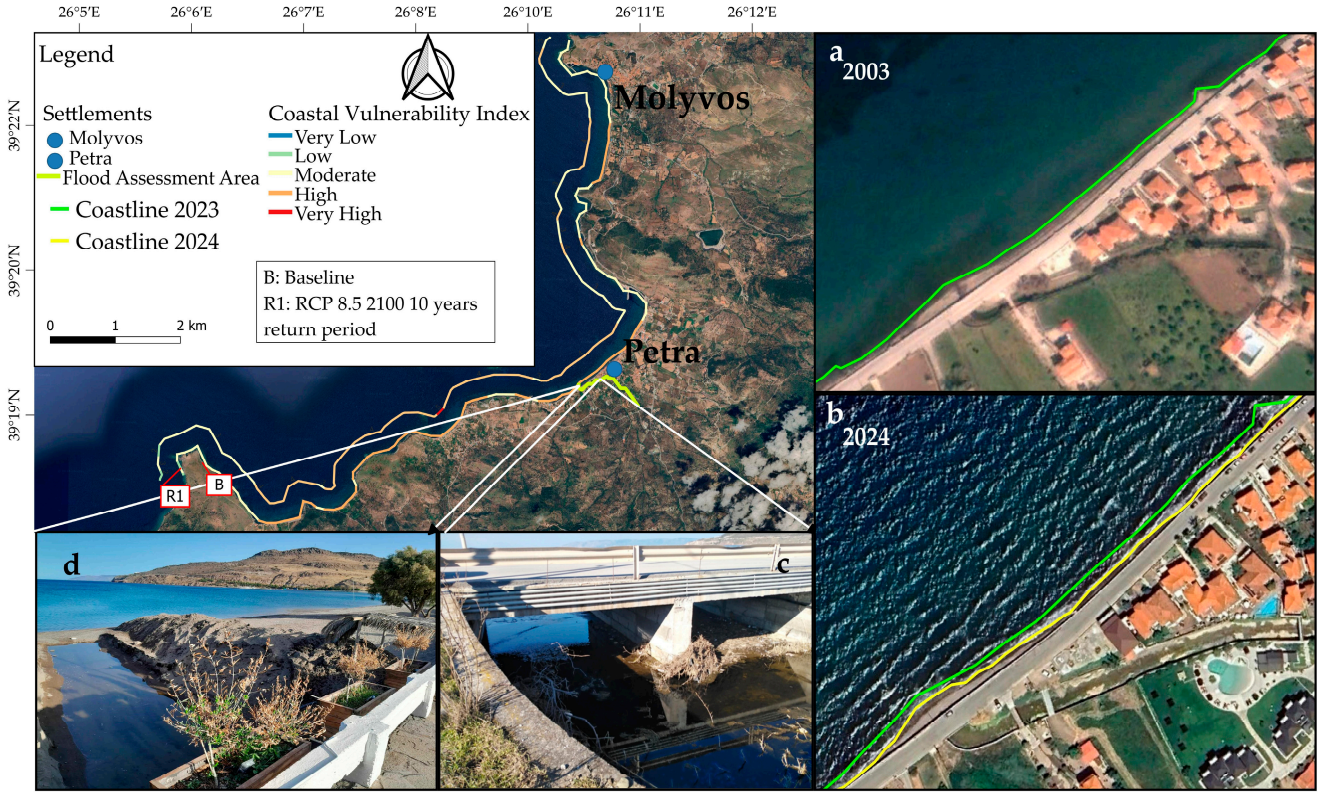


Figure 13. Impact of natural and human factors on the coast–watershed system in the area of interest: (**a**) coastline morphology adjacent to the Petra river's mouth in 2003 (Google Earth Image), (**b**) coastline morphology adjacent to the Petra river's mouth both in 2003 and 2024 (Google Earth Image), clearly illustrating beach retreat over these years, (**c**) human interventions (i.e., bridge, channelization) in the riverbed, and (**d**) human interventions in the river's mouth (Petra beach).

Overall, on Lesvos Island, the complex system of ephemeral streams that experience flooding in various parts feeds the coast with water and sediment during the flood events [12]. This scenario results in a negative sediment balance due to anthropogenic activities in the riverbed that obstruct sediment flow from the basin [11,16], thereby impeding coastal enrichment. Moreover, data and quantitative research are necessary to model anthropogenic actions in areas of interest [11]. The lack of data in watershed monitoring made it challenging to understand the behavior of the catchment. However, scientists argue that these challenges could develop an integrated framework strategy for touristic island coastal zones within intermitted coastal streams [11].

The "flexibility" of the regulatory framework regarding the coastal zone planning and the low motivation of the local communities to face the environmental issues of the coastal zone may be considered in combination with the technological solutions' adaptation. Island residents are aware of their share in beach erosion and deterioration, as well as of restoration measures [80].

5. Conclusions

Coastal erosion and changes in river watershed morphology, driven by both natural and human activities, reduce the river's sediment supply and coastal enrichment. This study proposes a comprehensive methodology for integrated coastal–watershed management in tourist destinations, offering valuable insights into the Petra–Molyvos coast and the role of the small coastal river in sediment enrichment. Despite the challenges of integrating flood risk and coastal vulnerability assessments—due to the complex interactions among driving processes, morphological responses, and risk receptors—combining coastal and river management effectively addresses changes in the coast–watershed system. The Petra

catchment functions as a sediment retainer, releasing only a limited amount to the coast of Petra–Molyvos. Consequently, the source of sediment supply to the shoreline is mainly the marine processes. However, human interventions in the Petra riverbed complicate shoreline replenishment, as materials are either not retained at the river mouth or are removed by residents.

A holistic approach is essential for understanding and managing the evolving patterns in the coast–watershed system. This approach requires establishing spatially distributed monitoring systems to address the limited geographical coverage of current efforts, enabling a more comprehensive analysis of how the system changes over time and across different locations. Challenges such as the lack of flow data, limited sediment yield information, and low-resolution relief data affect methods applied to small-scale sites. Further research is crucial to collect in situ data on marine and terrestrial observations, floodplain vegetation dynamics, anthropogenic interventions in the riverbed and mouth, and erosion monitoring. More information can be provided by verifying riparian and shoreline change by capturing high-accuracy images using unmanned aerial vehicles (UAVs).

Author Contributions: Conceptualization, T.H. and O.T.; methodology, S.P., I.S., A.G., S.S. and A.C.; software, A.G., S.S., A.C., I.S. and S.P.; validation, T.H. and O.T.; formal analysis, S.S., A.G. and I.S.; resources, S.P. and I.S.; data curation, S.S., A.G., I.S. and S.P.; writing—original draft preparation, S.P. and I.S.; writing—review and editing, S.P. and I.S.; review and editing, T.H., O.T. and G.V.; visualization, I.S., S.P. and A.G.; supervision, T.H. and O.T.; project administration, T.H.; funding acquisition, T.H. and O.T. All authors have read and agreed to the published version of the manuscript.

Funding: This work was supported by the research project BEACHTECH, co-funded by the European Union (ERDF) and national funds of Greece and Cyprus under the Cooperation Program "INTERREG V-A Greece-Cyprus 2014-2020", as well as by the project "Coastal Environment Observatory and Risk Management in Island Regions AEGIS+" implemented within the operational program "Competitiveness, Entrepreneurship and Innovation" (NSRF 2014-2020), co-financed by the Hellenic Government and the European Union (ERDF).

Data Availability Statement: The data used in this study are contained within the article. Additional data are available upon request from the corresponding author.

Acknowledgments: Part of the research was conducted by Papasarafianou Stamatia as a PhD candidate at the Science and Technology Department, University of Naples, Parthenope, Naples, Italy. Moreover, the authors would particularly like to thank T. Chatzivasileiou, student at the University of the Aegean, for his assistance in conducting the hydrological calculations required for the study.

Conflicts of Interest: The authors declare no conflict of interest.

References

1. Levrel, H.; Cabral, P.; Marcone, O.; Mongruel, R. The services provided by marine ecosystems. In *Value and Economy of Marine Resources*; John Wiley & Sons Inc.: Hoboken, NJ, USA, 2014; pp. 1–51.
2. Monioudi, I.N.; Velegrakis, A.F.; Chatzipavlis, A.E.; Rigos, A.; Karambas, T.; Vousdoukas, M.I.; Hasiotis, T.; Koukourouvli, N.; Peduzzi, P.; Manoutsoglou, E.; et al. Assessment of island beach erosion due to sea level rise: The case of the Aegean archipelago (Eastern Mediterranean). *Nat. Hazards Earth Syst. Sci.* **2017**, *17*, 449–466. [CrossRef]
3. Andreadis, O.; Chatzipavlis, A.; Hasiotis, T.; Monioudi, I.; Manoutsoglou, E.; Velegrakis, A. Assessment of and Adaptation to Beach Erosion in Islands: An Integrated Approach. *J. Mar. Sci. Eng.* **2021**, *9*, 859. [CrossRef]
4. Ai, B.; Tian, Y.; Wang, P.; Gan, Y.; Luo, F.; Shi, Q. Vulnerability Analysis of Coastal Zone Based on InVEST Model in Jiaozhou Bay, China. *Sustainability* **2022**, *14*, 6913. [CrossRef]
5. Pantusa, D.; D'Alessandro, F.; Frega, F.; Francone, A.; Tomasicchio, G.R. Improvement of a coastal vulnerability index and its application along the Calabria Coastline, Italy. *Sci. Rep.* **2022**, *12*, 21959. [CrossRef] [PubMed]
6. Tan, W.J.; Yang, C.F.; Chateau, P.A.; Lee, M.T.; Chang, Y.C. Integrated coastal zone management for sustainable tourism using a decision support system based on system dynamics: A case study of Cijin, Kaohsiung, Taiwan. *Ocean. Coast. Manag.* **2018**, *153*, 131–139. [CrossRef]
7. Monioudi, I.N.; Velegrakis, A.F.; Chatzistratis, D.; Vousdoukas, M.I.; Savva, C.; Wang, D.; Bove, G.; Mentaschi, L.; Paprotny, D.; Morales-Nápoles, O.; et al. Climate change—Induced hazards on touristic island beaches: Cyprus, Eastern Mediterranean. *Front. Mar. Sci.* **2023**, 10. [CrossRef]

8. SETE. Association of the Greek Touristic Businesses, International Airline Arrivals: 2015 & Planning Report (Slots). 2016. Available online: http://sete.gr/media/4629/ypa-2015-and-slots-2016.pdf (accessed on 20 May 2021).
9. ECLAC. *An Assessment of the Economic Impact of Climate Change on the Transportation Sector in Barbados*; UN Economic Commission for Latin America and the Caribbean ECLAC Technical Report LC/CAR/L309; ECLAC: Santiago de Chile, Chile, 2011; 44p.
10. Tzoraki, O.; Monioudi, I.; Velegrakis, A.; Moutafis, N.; Pavlogeorgatos, G.; Kitsiou, D. Resilience of touristic island beaches under sea level rise: A methodological framework. *Coast. Manag.* **2018**, *46*, 78–102. [CrossRef]
11. Malara, G.; Zema, D.A.; Arena, F.; Bombino, G.; Zimbone, S.M. Coupling watershed—Coast systems to study evolutionary trends: A review. *Earth Sci. Rev.* **2020**, *201*, 103040. [CrossRef]
12. Samaras, A.G.; Koutitas, C.G. Modeling the impact on coastal morphology of the water management in transboundary river basins: The case of River Nestos. *Manag. Environ. Qual. Int. J.* **2008**, *19*, 455–466. [CrossRef]
13. Sharp, R.; Douglass, J.; Wolny, S.; Arkema, K.; Bernhardt, J.; Bierbower, W.; Chaumont, N.; Denu, D.; Fisher, D.; Glowinski, K.; et al. *InVEST 3.9.1 User's Guide*; The Natural Capital Project; Stanford University; University of Minnesota; The Nature Conservancy; World Wildlife Fund: Stanford, CA, USA, 2020.
14. Papasarafianou, S.; Gkaifyllia, A.; Iosifidi, A.-E.; Sahtouris, S.; Wulf, N.; Culibrk, A.; Stamataki, M.-D.; Chatzivasileiou, T.; Siarkos, I.; Rouvenaz, C.; et al. Vulnerability of small rivers coastal part due to floods: The case study of Lesvos North-West coast. *Environ. Sci. Proc.* **2023**, *25*, 44. [CrossRef]
15. Salomons, W. Sediments in the Catchment-coast Continuum. *J. Soils Sediments* **2005**, *5*, 2–8. [CrossRef]
16. Velegrakis, A.F.; Vousdoukas, M.; Meligonitis, R. Erosion of Islandic beaches: Phenomenology and causes of the degradation of the largest natural resource of isclandic Greece. In *Islandic Greece in the 21st Century*; Tsaltas, G., Ed.; Sideris Publications: Athens, Greece, 2005; pp. 243–262. (In Greek)
17. Nasr, A.A.; Wahl, T.; Rashid, M.M.; Camus, P.; Haigh, I.D. Assessing the dependence structure between oceanographic, fluvial, and pluvial flooding drivers along the United States coastline. *Hydrol. Earth Syst. Sci.* **2021**, *25*, 6203–6222. [CrossRef]
18. Hasiotis, T.; Andreadis, O.; Chatzipavlis, A.; Mettas, C.; Evagorou, E.; Kountouri, J.; Hadjimitsis, D.; Christofi, D.; Loizidou, M.; Chrysostomou, G. A holistic high resolution monitoring approach in studying coastal erosion of a highly touristic beach, Coral Bay, Cyprus. In Proceedings of the Ninth International Conference on Remote Sensing and Geoinformation of the Environment (RSCy2023), Ayia Napa, Cyprus, 3–5 April 2023; SPIE: Bellingham, WA, USA, 2023; Volume 12786, p. 1278611. [CrossRef]
19. Velegrakis, A.F.; Vousdoukas, M.; Andreadis, E.P.; Adamakis, G.; Meligonitis, R. Impacts of dams on their downstream beaches: A case study from Eresos coastal basin, island of Lesvos, Greece. *Mar. Georesour. Geotechnol.* **2008**, *24*, 350–371. [CrossRef]
20. Samaras, A.G.; Koutitas, C.G. Modeling the impact of climate change on sediment transport and morphology in coupled watershed-coast systems: A case study using an integrated approach. *Int. J. Sediment Res.* **2014**, *29*, 304–315. [CrossRef]
21. Hammar-Klose, E.S.; Thieler, E.R. *Coastal Vulnerability to Sea-Level Rise: A Preliminary Database for the U.S. Atlantic, Pacific, and Gulf of Mexico Coasts*; U.S. Geological Survey: Reston, VA, USA, 2001.
22. Prinos, P. Review of Food Hazard Mapping. Integrated Flood Risk Analysis and Management Methodologies. Spain. April 2008. Available online: https://www.floodsite.net (accessed on 18 June 2019).
23. Toimil, A.; Díaz-Simal, P.; Losada, I.J.; Camus, P. Estimating the risk of loss of beach recreation value under climate change. *Tour. Manag.* **2018**, *68*, 387–400. [CrossRef]
24. Olsen, S.; Tobey, J.; Kerr, M. A common framework for learning from ICM experience. *Ocean. Coast. Manag.* **1997**, *37*, 155–174. [CrossRef]
25. Cicin-Sain, B.; Belfiore, S. Linking marine protected areas to integrated coastal and ocean management: A review of theory and practice. *Ocean. Coast. Manag.* **2005**, *48*, 847–868. [CrossRef]
26. Sajjad, M.; Li, Y.; Tang, Z.; Cao, L.; Liu, X. Assessing Hazard Vulnerability, Habitat Conservation, and Restoration for the Enhancement of Mainland China's Coastal Resilience. *Earth's Future* **2018**, *6*, 326–338. [CrossRef]
27. Salomons, W.; Kremer, H.H.; Turner, R.K.; Andreeva, E.N.; Arthurton, R.S.; Behrendt, H.; Burbridge, P.; Chen, C.-T.A.; Crossland, C.J.; Gandrass, J.; et al. The Catchment to Coast Continuum. In *Coastal Fluxes in the Anthropocene: The Land-Ocean Interactions in the Coastal Zone*, 2nd ed.; Crossland, C.J., Kremer, H.H., Lindeboom, H.J., Marshall Crossland, J.I., Le Tissier, M.D.A., Eds.; Springer: Berlin/Heidelberg, Germany, 2005; pp. 145–200. [CrossRef]
28. Pollard, J.; Spencer, T.; Brooks, S. The interactive relationship between coastal erosion and flood risk. *Prog. Phys. Geogr.* **2019**, *43*, 574–585. [CrossRef]
29. Alves, B.; Angnuureng, D.; Morand, P.; Alma, R. A review on coastal erosion and flooding risks and best management practices in West Africa: What has been done and should be done. *J. Coast. Conserv.* **2020**, *24*, 38. [CrossRef]
30. Hellenic Statistical Authority (HSA). Tables of Demographic and Social Characteristics of the Resident Population of Greece (2011 Population-Housing Census). 2011. Available online: https://www.statistics.gr/en/home (accessed on 20 March 2014).
31. Monioudi, I.N.; Karditsa, A.; Chatzipavlis, A.; Alexandrakis, G.; Andreadis, O.; Velegrakis, A.F.; Poulos, S.; Ghionis, G.; Petrakis, S.; Sifnioti, D.; et al. Assessment of the vulnerability of the eastern Cretan beaches (Greece) to sea level rise. *Reg. Environ. Chang.* **2016**, *16*, 1951–1962. [CrossRef]
32. Vacchi, M.; Rovere, A.; Zouros, N.; Desruelles, S.; Caron, V.; Firpo, M. Spatial distribution of sea-level markers in Lesvos Island (NE Aegean Sea): Evidence of differential relative sea-level changes and the neotectonic implications. *Geomorphology* **2012**, *159–160*, 50–62. [CrossRef]

33. Saroglou, H. Engineering geological behavior of volcanic formations. References to instability phenomena and town planning in Lesvos Island, Greece. *Bull. Geol. Soc. Greece* **2012**, *46*, 108–122. [CrossRef]
34. National Institute of Geological and Mining Research (NIGMR). *Geological Map of Greece. Lesbos Island. 1:50,000 (Five Sheets)*; NIGMR: Athine, Greece, 1975.
35. Zouros, N. Assessment, protection, and promotion of geomorphological and geological sites in the Aegean area, Greece. *Géomorphol. Relief Process. Environ.* **2005**, *11*, 227–234. [CrossRef]
36. Zouros, N.; Pavlides, S.; Soulakellis, N.; Chatzipetros, A.; Vasileiadou, K.; Valiakos, I.; Mpentana, K. Using active fault studies for raising public awareness and sensitization on seismic hazards: A case study from Lesvos petrified forest Geopark, NE Aegean Sea. *Geoheritage* **2011**, *3*, 317–327. [CrossRef]
37. Delattre, L.; Debolini, M.; Paoli, J.; Napoleone, C.; Moulery, M.; Leonelli, L.; Santucci, P. Understanding the relationships between extensive livestock systems, land-cover changes, and cap support in less-favored Mediterranean areas. *Land* **2020**, *9*, 518. [CrossRef]
38. Dimopoulos, T.; Helfenstein, J.; Kreuzer, A.; Mohr, F.; Sentas, S.; Giannelis, R.; Kizos, T. Different responses to mega-trends in less favorable farming systems. Continuation and abandonment of farming land on the islands of Lesvos and Lemnos, Greece. *Land Use Policy* **2023**, *124*, 106435. [CrossRef]
39. Namara, W.G.; Damisse, T.A.; Tufa, F.G. Application of HEC-RAS and HEC-GeoRAS model for Flood Inundation Mapping, the case of Awash Bello Flood Plain, Upper Awash River Basin, Oromiya Regional State, Ethiopia. *Model. Earth Syst. Environ.* **2022**, *8*, 1449–1460. [CrossRef]
40. Traore, V.B.; Bop, M.; Faye, M.; Malomar, G.; Gueye, E.O.; Sambou, H.; Dione, A.N.; Fall, S.; Tahirou Diaw, A.; Sarr, J.; et al. Using of Hec-ras Model for Hydraulic Analysis of a River with Agricultural Vocation: A Case Study of the Kayanga River Basin, Senegal. *Am. J. Water Res.* **2015**, *3*, 147–154. [CrossRef]
41. Nkeki, F.N.; Bello, E.I.; Agbaje, I.G. Flood risk mapping and urban infrastructural susceptibility assessment using a GIS and analytic hierarchical raster fusion approach in the Ona River Basin, Nigeria. *Int. J. Disaster Risk Reduct.* **2022**, *77*, 103097. [CrossRef]
42. Topouzelis, K.; Makri, D.; Stoupas, N.; Papakonstantinou, A.; Katsanevakis, S. Seagrass mapping in Greek territorial waters using Landsat-8 satellite images. *Int. J. Appl. Earth Obs. Geoinf.* **2018**, *67*, 98–113. [CrossRef]
43. Monioudi, I.; Velegrakis, A.F. *Toolbox Manual—Wind and Wave Data Analysis GUI Manual*; Department of Marine Sciences, School of Environment, University of Aegean: Mytilene, Greece, 2015.
44. Vousdoukas, M.; Mentaschi, L.; Voukouvalas, E.; Verlann, M.; Jevrejeva, S.; Jackson, L.P.; Feyen, L. Global probabilistic projections of extreme sea levels show intensification of coastal flood hazard. *Nat. Commun.* **2018**, *9*, 2360. [CrossRef] [PubMed]
45. Komar, P.D. *Beach Processes and Sedimentation*; Prentice Hall: Upper Saddle River, NJ, USA, 1998.
46. Koutitas, X.G. *Introduction to Coastal Engineering and Port Works*; Ziti Publication: Thessaloniki, Greece, 1994. (In Greek)
47. Helmi, A.M. Quantifying catchments sediment release in arid regions using GIS-based Universal soil loss equation (USLE). *Ain Shams Eng. J.* **2023**, *8*, 102038. [CrossRef]
48. Kaffas, K.; Pisinaras, V.; Al Sayah, M.J.; Santopietro, S.; Righetti, M. A USLE-based model with modified LS-factor combined with sediment delivery module for Alpine basins. *Catena* **2021**, *207*, 105655. [CrossRef]
49. Bezak, N.; Mikos, M.; Borrelli, P.; Alewell, C.; Alvarez, P.; Anache, J.A.; Baartman, J.; Ballabio, C.; Biddoccu, M.; Cerdà, A.; et al. Soil erosion modeling: A bibliometric analysis. *Environ. Res.* **2021**, *197*, 111087. [CrossRef]
50. Todisco, F.; Vergni, L.; Ortenzi, S.; Di Matteo, L. Soil Loss Estimation Coupling a Modified USLE Model with a Runoff Correction Factor Based on Rainfall and Satellite Soil Moisture Data. *Water* **2022**, *14*, 2081. [CrossRef]
51. Benavidez, R.; Jackosn, B.; Maxwell, D.; Norton, K. A review of the (Evised) Universal Soil Loss Equation ((R) USLE): With a view to increasing its global applicability and improving soil loss estimates. *Hydrol. Earth Syst. Sci.* **2018**, *22*, 6059–6086. [CrossRef]
52. Rozos, D.; Skilodimou, H.; Loupasakis, C.; Bathrellos, G. Application of the revised universal soil loss equation model on landslide prevention. An example from N. Euboea (Evia) Island, Greece. *Environ. Earth Sci.* **2013**, *70*, 3255–3266. [CrossRef]
53. Michas, S.; Nikolaou, K.; Koukouvinos, A.; Mamassis, N. *Estimation of Sediment Yield with MUSLE and Monitoring. A Case Study for Tsiknias Dam at Lesvos Island in Greece*; IWA Balkan Young Water Professionals: Thessaloniki, Greece, 2015; p. 8.
54. Vachaviolos, T. Estimation of Soil Erosion, Sediment Yield and Reservoir Sedimentation from Empirical Methods with Emphasis on Rainfall's Effect. Master's Thesis, National Technical University of Athens, Athens, Greece, 2014.
55. Alves, W.S.; Martins, A.P.; Morrais, W.A.; Possa, E.M.; Castro, R.M.; Borges de Moura, D.M. USLE modeling of soil loss in a Brazilian cerrado catchment. *Remote Sens. Appl. Soc. Environ.* **2022**, *27*, 100788. [CrossRef]
56. Panagos, P.; Meusburger, K.; Alewell, C.; Montanarella, L. Soil erodibility estimation using LUCAS point survey data of Europe. *Environ. Model. Softw.* **2012**, *30*, 143–145. [CrossRef]
57. Van der Knijff, J.M.; Jones, R.J.A.; Montanarella, L. *Soil Erosion Risk Assessment in Europe*; JRC Scientific and Technical Report—EUR 19022 EN; European Soil Bureau; European Commission: Brussels, Belgium, 2000.
58. Van der Knijff, J.M.; Jones, R.J.A.; Montanarella, L. *Soil Erosion Risk Assessment in Italy*; JRC Scientific and Technical Report—EUR 19044 EN; European Soil Bureau; European Commission: Brussels, Belgium, 2000.
59. Mitasova, H.; Mitas, L. Modelling Physical Systems. In *Geographic Information Systems and Environmental Modelling*; Parks, B., Crane, M., Clarke, K., Eds.; Prentice Hall: Upper Saddle River, NJ, USA, 2001.

60. Zarris, D.; Lykoudi, E. Prediction of soil erosion at risk areas of the island Kefalonia using the USLE equation. In Proceedings of the 6th Panhellenic Conference of the Greek Geographic Company, Thessaloniki, Greece, 3–6 October 2002; Volume 2, pp. 412–419.
61. Vanoni, V.A. Sedimentation engineering. In *Manuals and Reports on Engineering Practice*; American Society of Civil Engineers: New York, NY, USA, 1975.
62. U.S. Army Corps of Engineers. HEC-RAS River Analysis System. In *User's Manual, Version 6.0*; US Army Corps of Engineers; Institute for Water Resources Hydrologic Engineering Center: Davis, CA, USA, 2021. Available online: https://www.hec.usace.army.mil/software/hec-ras/documentation/HEC-RAS_6.0_Users_Manual.pdf (accessed on 20 May 2021).
63. Beven, K.J. *Rainfall-Runoff Modelling: The Primer*; Wiley-Blackwell: Oxford, UK, 2012.
64. Michailidi, E.M.; Antoniadi, S.; Koukouvinos, A.; Bacchi, B.; Efstratiadis, A. Timing the time of concentration: Shedding light on a paradox. *Hydrol. Sci. J.* **2018**, *63*, 721–740. [CrossRef]
65. Campos, J.N.B.; de Carvalho Studart, T.M.; de Assis de Souza Filho, F.; Costa Porto, V. On the Rainfall Intensity–Duration–Frequency Curves, Partial-Area Effect and the Rational Method: Theory and the Engineering Practice. *Water* **2020**, *12*, 2730. [CrossRef]
66. Lapides, D.A.; Sytsma, A.; Thompson, S. Implications of Distinct Methodological Interpretations and Runoff Coefficient Usage for Rational Method Predictions. *J. Am. Water Resour. Assoc.* **2021**, *57*, 859–874. [CrossRef]
67. Xafoulis, N.; Farsirotou, E.; Kotsopoulos, S.; Alamanis, N. Flood hazard assessment in a mountainous river basin in Thessaly, Greece, Based on 1D/2D numerical simulation. *Energy* **2022**, *8*, 100142. [CrossRef]
68. Daniil, E.I.; Michas, S.N.; Nikolaou, K.; Lazaridis, L.S. Systematic Approach for ungagged basins' discharge determination in western Peloponnese, Greece. *Glob. NEST J.* **2012**, *14*, 344–353.
69. Daniil, E.I.; Michas, S.N.; Aerakis, G. Hydrologic issues in demarcation studies of watercourses in Greece. In Proceedings of the 15th International Conference on Environmental Science and Technology, CEST 2017, Rhodes, Greece, 31 August–2 September 2017.
70. Young, C.B.; McEnroe, B.M.; Rome, A. Empirical Determination of Rational Method Runoff Coefficients. *J. Hydrol. Eng.* **2009**, *14*, 1283–1289. [CrossRef]
71. Dhakal, N.; Fanf, X.; Cleveland, T.G.; Thompson, D.B. Revisiting Modified Rational Method. In *World Environmental and Water Resources Congress 2011: Bearing Knowledge for Sustainability*; ASCE: New York, NY, USA, 2011.
72. Carey, B.W.; Stone, B.; Norman, P.L.; Shilton, P. Chapter 4: The empirical version of the rational method. In *Soil Conservation Guidelines for Queensland*; Department of Science, Information Technology and Innovation: Brisbane, Australia, 2015.
73. Baiamonte, G. A rational runoff coefficient for a revisited rational formula. *Hydrol. Sci. J.* **2020**, *65*, 112–126. [CrossRef]
74. Special Secretariat for Water. *Flood Risk Management Plan, River Basin Districts of the Aegean Islands (Northern and Southern Aegean)*; Government Gazette approving the 1st Revision of RBMP for the Aegean Islands RBD: 4677/B/29.12.2017; Ministry of Environment and Energy, Special Secretariat for Water: Athens, Greece, 2018.
75. Shah, H.F.; Alam, A.; Bhat, S.M.; Ahmad, S. One Dimensional Steady Flow Analysis Using HEC-RAS—A Case of River Jhelum, Jammu, and Kashmir. *Eur. Sci. J.* **2016**, *12*, 1857–7881.
76. Cook, A.; Merwade, V. Effect of topographic data, geometric configuration and modeling approach on flood inundation mapping. *J. Hydrol.* **2009**, *377*, 131–142. [CrossRef]
77. Nharo, T.; Makurira, H.; Gumindoga, W. Mapping floods in the middle Zambezzi Basin using earth observation and hydrological modeling techniques. *Phys. Chem. Earth* **2019**, *114*, 102787. [CrossRef]
78. Culbrik, A.; Tzoraki, O.; Portman, M.E. Adaptation of a freshwater evaluation framework to a coastal system: The case of Kamari, Santorini. *J. Environ. Manag.* **2021**, *288*, 112406. [CrossRef] [PubMed]
79. Nones, M. Dealing with sediment transport in flood risk management. *Acta Geophys.* **2019**, *67*, 677–685. [CrossRef]
80. Tourlioti, P.N.; Portman, M.E.; Tzoraki, O.; Pantelakis, I. Interacting with the coast: Residents' knowledge and perceptions about coastal erosion (Mytilene, Lesvos Island, Greece). *Ocean Coast. Manag.* **2021**, *210*, 105705. [CrossRef]

Disclaimer/Publisher's Note: The statements, opinions and data contained in all publications are solely those of the individual author(s) and contributor(s) and not of MDPI and/or the editor(s). MDPI and/or the editor(s) disclaim responsibility for any injury to people or property resulting from any ideas, methods, instructions or products referred to in the content.